https://doi.org/10.5194/egusphere-2026-2838
Preprint. Discussion started: 28 July 2026

Novel mobile measurements of ammonia and methane: distinguishing agricultural and traffic sources in the Netherlands

Jun Zhang[1]*, Arjan Hensen[1]*, Baye Thera[1],
Pim van den Bulk[1], Daniëlle van Dinther[1], Ilona Velzeboer[1],
Enrico Dammers[2], Gerrit Jan de Bruin[1], Paula Bronsveld[1], Martijn Schaap[2]

[1]Environmental Modelling, Sensing & Analysis, TNO, Petten, 1755 LE, the Netherlands
[2]Air Quality and Emissions Research, TNO, Utrecht, 3584 CB, the Netherlands
Correspondence to: Jun Zhang (jun.zhang@tno.nl); Arjan Hensen (arjan.hensen@tno.nl)

Abstract. A mobile atmospheric measurement platform combining an open-path ammonia (NH_3) analyzer (HT-8700E) and a closed-path tunable infrared laser direct absorption spectroscopy (TILDAS) multi-gas system was deployed to enable simultaneous, high-frequency observations of NH_3, methane (CH_4), and carbon monoxide (CO) under real-world conditions. The open-path configuration minimizes inlet-related artefacts and enables fast-response NH_3 measurements. A comprehensive measurement framework is presented, including instrument integration, field calibration and validation using co-located reference measurements, data synchronization, plume identification, background removal, and plume-integrated enhancement analysis.

The performance of the platform was evaluated during a 160 km mobile campaign in the Veluwe region of the Netherlands, a Natura 2000 nature reserve surrounded by intensive livestock farming. During the campaign, plumes from 49 individual sources and approximately 630 transient traffic-related events were detected, resolving short-lived concentration enhancements across agricultural, industrial, and traffic-dominated environments. Plume-integrated enhancement ratios (ΣNH_3:ΣCH_4) showed systematic differences among source types, with low ratios for livestock farms (~0.04 for cattle and goats), intermediate values for industrial sources, and substantially higher ratios for manured fields (>2) and traffic plumes (>4). In addition, NH_3 emission factors derived for traffic increased with driving speed from approximately 0.12 g kg^{-1} fuel at low speeds to ~0.28 g kg^{-1} under highway conditions.

These results demonstrate that simultaneous mobile measurements of NH_3, CH_4, and CO provide an effective approach for detecting and differentiating emission sources under real-world conditions. The combined observations reveal distinct source signatures and potential gaps in existing emission inventories. Although uncertainties remain due to atmospheric variability, calibration, limited temporal sampling, and overlap in source-specific ratios, the methodology shows strong potential for high-resolution characterization of heterogeneous NH_3 emissions through repeated mobile monitoring campaigns.

https://doi.org/10.5194/egusphere-2026-2838
Preprint. Discussion started: 28 July 2026

1 Introduction

Ammonia (NH_3) emissions are a major contributor to reactive nitrogen (Nr) deposition in the Netherlands, driving eutrophication, biodiversity loss, and potential human health impacts. NH_3 emission densities are among the highest in Europe (Wever et al., 2024), with livestock production, fertilizer application, and traffic representing the primary sources. However, emission estimates largely rely on bottom-up inventories rather than direct measurements, and especially at local scale substantial uncertainties remain due to the heterogeneity in sources and practices, as well as atmospheric dispersion, chemical transformation, and deposition processes (Ding et al., 2024; Kumar et al., 2025; Nair & Yu, 2020). The availability of high-resolution NH_3 measurements are therefore essential for verifying emission inventories, evaluating emission reduction strategies and supporting evidence-based policy decisions.

Traditionally, NH_3 monitoring in the Netherlands relies mainly on fixed stations, primarily located in sensitive natural areas (Van Pul et al., 2004), complemented by a limited number of sites with high-time-resolution measurements within the national air quality monitoring network Landelijk Meetnet Luchtkwaliteit (LML) (Van Zanten et al., 2017). While these networks provide valuable long-term observations, their spatial coverage is insufficient to resolve local emission hotspots or distinguish individual source types. More recently, some studies in intensive agricultural regions have applied periodical monitoring approaches, including passive samplers, to characterize NH_3 levels in source areas (Lô et al., 2025; Van Wijk et al., 2025). However, their temporal resolution is typically limited to monthly averages, which hampers deriving emission information for individual sources or specific source types (Li et al., 2025). Satellite observations offer broader spatial coverage but lack the spatial resolution required to resolve near-source emissions or verify source-specific contributions (Ding et al., 2024).

Over the past decades, mobile measurement platforms have been widely used to quantify emissions of greenhouse gases such as methane (CH_4) and nitrous oxide (N_2O) from point and area sources using inverse modelling approach (Mønster et al., 2014; Moyes et al., 2025; Yacovitch et al., 2015; Yang et al., 2025). Building on this foundation, a few studies have extended mobile approaches to on-road NH_3 emission quantification, using open-path and portable spectroscopic techniques to derive NH_3 emission factors under real-world driving conditions (Dai et al., 2024; Suarez-Bertoa et al., 2015; Sun et al., 2014).

Mobile NH_3 measurements provide a promising pathway to overcome the limitations of fixed and low-resolution monitoring. Earlier mobile applications using wet-chemical or closed-path optical analyzers were constrained by slow response times and adsorption artifacts (Twigg et al., 2022), but recent advances in high-frequency open-path optical techniques have largely addressed these challenges, enabling real-time NH_3 measurements in emission-dense environments (Pu et al., 2023; Sun et al., 2014). The HT-8700E NH_3 analyzer (Healthy Photon Co., Ltd., China) employs a quantum cascade laser combined with an open-path Herriott cell, allowing fast-response mobile NH_3 measurements without inlet line interactions. When coupled with high-resolution analyzers for CH_4, N_2O, carbon dioxide (CO_2), and carbon mono-oxide (CO), this system enables simultaneous characterization of NH_3 and greenhouse gas emissions. Similar HT-based mobile platforms have been successfully deployed in the United States (Golston et al., 2020; Vechi et al., 2023) and China (Sun et al., 2014, 2017), demonstrating their ability to resolve agricultural and traffic emissions at fine spatial and temporal scales.

https://doi.org/10.5194/egusphere-2026-2838
Preprint. Discussion started: 28 July 2026

In this study, we report the first European mobile deployment of the commercial HT-8700E analyzer, focusing on the Veluwe region, a mixed agricultural landscape and nature reserve (Natura 2000) in the central Netherlands. The objectives are to: (1) demonstrate the capability of mobile NH_3 observations to resolve spatial and temporal variability of emissions, (2) identify and characterize agricultural and non-agricultural emission sources using simultaneous NH_3, CH_4, CO and CO_2 measurements, (3) support the quantification of NH_3 emissions from livestock farms by analyzing NH_3:CH_4 ratios, and (4) estimate traffic NH_3 emission factors from NH_3:CO_x (CO_2 and CO) ratios. This approach provides a novel measurement framework for regional NH_3 source characterization and supports improved emission assessment and interpretation.

2 Methodology

2.1 Study Area

Agriculture is the dominant source of NH_3 emissions in the Netherlands, accounting for 91% of the national total (116.4 Gg NH_3 yr^{-1} in 2023) (Statistics Netherlands (CBS), 2024). In Gelderland province, where the Veluwe is located, emission densities reach 9–12 t km^{-2} yr^{-1}, roughly three to four times higher than the national average (2.9 t km^{-2} yr^{-1}) (Dutch National Institute for Public Health and the Environment [RIVM] & CBS, 2024), reflecting the high density of livestock farms and spatial heterogeneity of agricultural sources in the area.

The Veluwe, the largest nature reserve in the Netherlands (~88,400 ha), is a protected Natura 2000 site with predominantly coniferous forests, along with heathlands, deciduous forests, and sandy soils. Despite its protected status (European Environment Agency (EEA), 2023), nitrogen deposition remains elevated, with average levels of ~1,445 mol N ha^{-1} yr^{-1} (range ~1,000–1,860 mol N ha^{-1} yr^{-1}) and locally exceeding 2,000 mol N ha^{-1} yr^{-1} in downwind regions such as the western Veluwe, exceeding critical loads for many habitat types (RIVM, 2023).

The Veluwe is bordered to the west and southwest by the Gelderse Vallei, an intensive agricultural region with substantial emissions from livestock farming and manure application (Fig. 1). In addition, traffic contributes to local NH_3 levels, with several motorways crossing the reserve and surrounding urban areas generating road-related emissions (Fig. 1). Although generally lower than agricultural sources, traffic-related NH_3 emissions can be locally significant, yet on-road quantification of these contributions remains limited (Chen et al., 2022; Wen et al., 2023).

https://doi.org/10.5194/egusphere-2026-2838
Preprint. Discussion started: 28 July 2026

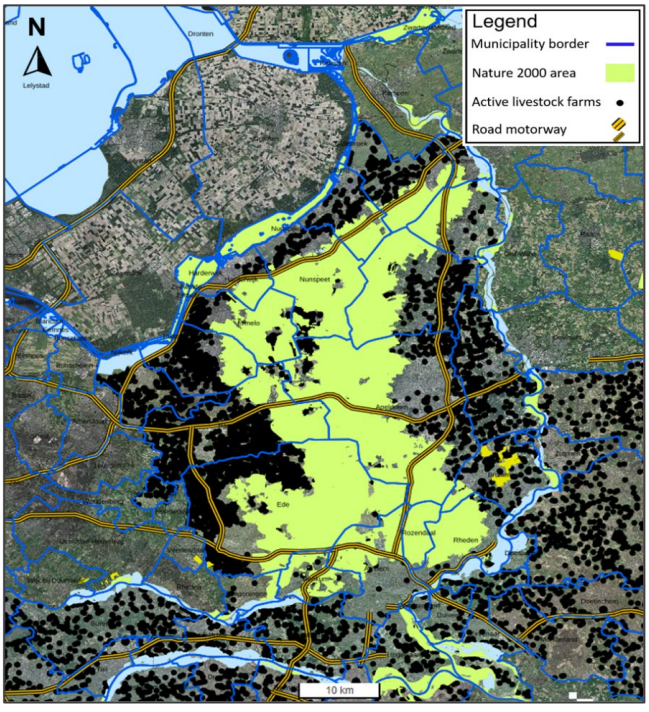

Figure 1: Map of the study area in Gelderland province, the Netherlands, highlighting livestock farms, major motorways, and the Natura 2000 protected area. Modified from base map data provided by the Province Gelderland public map viewer (Rijksdienst voor Ondernemend Nederland, n.d.-a).

2.2 Measurement setup and campaign

2.2.1 Measurement setup

Data were collected using a mobile laboratory truck (Fig. 2a) equipped with a closed-path tunable infrared laser direct absorption spectroscopy (TILDAS) quantum cascade laser (QCL)-based multi-gas analyzer (Aerodyne, USA), which simultaneously measured CH_4, ethane (C_2H_6), N_2O, CO, CO_2, and water vapour (H_2O) at 2 Hz. The system achieved measurement precisions of 2.4 ppb for CH_4, 0.1 ppb for C_2H_6, 0.1 ppb for N_2O, 2.5 ppb for CO, and 0.4 ppm for CO_2 (Tong et al., 2025). To minimize contamination from the vehicle's own exhaust, the analyzer inlet was connected to a 6 m stainless steel sampling line extending 1.5m ahead of the trailer and positioned ~3 m above ground level, well upstream of the exhaust outlet. The measurement system included a central data acquisition computer, Wi-Fi router, and GPS unit, all powered by a battery pack. The TILDAS instrument was calibrated at the beginning and end of each measurement day using calibration gases referenced to WMO-certified standards at the Cabauw tall tower, the ICOS atmospheric measurement station in the Netherlands (Delre et al., 2022; Velzeboer et al., 2024).

To enable high-frequency NH_3 measurements, the mobile platform was equipped with an open-path NH_3 analyzer (HT-8700E, Healthy Photon Co., Ltd., China, hereafter, HT) mounted on the roof of the truck tractor (Fig. 2a).

https://doi.org/10.5194/egusphere-2026-2838
Preprint. Discussion started: 28 July 2026

The instrument measures NH_3 concentrations at up to 10 Hz with an accuracy of ~0.15 ppb (Wang et al., 2021). The open-path configuration avoids inlet-related adsorption and memory effects that commonly affect closed-path NH_3 measurements, enabling fast-response detection of short-lived concentration enhancements in mobile applications.

All measurement data were averaged to 1 Hz. GPS, TILDAS, and HT datasets were synchronized by applying a 5-s correction to account for the TILDAS inlet line delay. Meteorological data, including wind speed and direction, were obtained from the Royal Netherlands Meteorological Institute (KNMI) station at Deelen Airport, located 19 km from the southern edge of the Veluwe. In addition, a 3-D sonic anemometer (model Gill WindMasterPro™, Gill Instruments, Lymington, UK) was deployed outside the mobile laboratory to perform short-duration measurements at selected locations along the driving route, providing on-site verification of ground-level wind conditions.

2.2.2 Measurement campaign

The functioning of the mobile platform was demonstrated during a 160 km long mobile measurement campaign on 21 February 2023. Measurements started at 09:00 UTC in the Veluwe region and were conducted at an average driving speed ~65 km h^{-1}. Wind speed remained relatively constant at 3–4 m s^{-1}, with a predominantly southwesterly direction (220–240°), typical for the region. Weather conditions were cloudy in the morning, with occasional rain showers beginning after 13:00 UTC. The HT mirrors were manually cleaned following initial rain, and measurements were terminated after 13:20 UTC when a prolonged rain period started. The route was chosen such that different agricultural regions to the west and north of the nature areas were covered, as well as some agricultural areas enclosed by the nature area. By driving through the nature area a regional background condition was sampled. The route and the measured variation in NH_3 concentrations along the route are shown in Fig. 2b. Additional observations of traffic-related emissions were made along Highway A1 between Hilversum and Amsterdam on the same day between 15:00 and 15:45 UTC during rainless conditions and at a driving speed of ~80 km h^{-1} (see Fig. S1 in the Supplement).

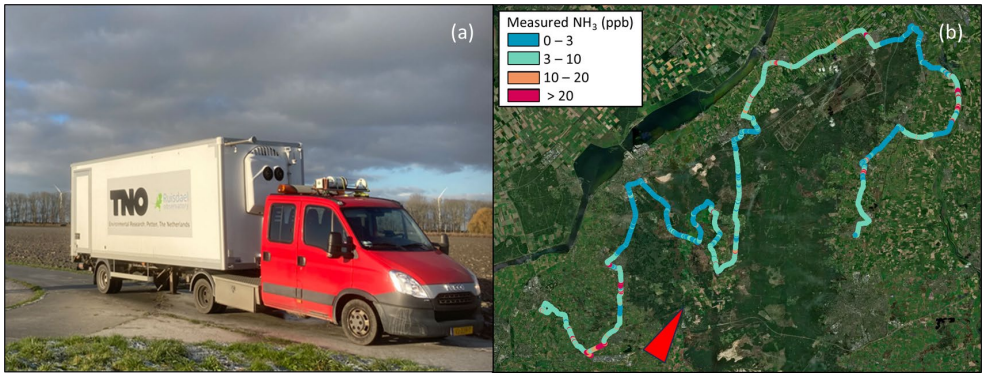

Figure 2: (a) The mobile measurement platform equipped with the HT open-path NH_3 analyzer mounted on the roof of the truck. The inlet of the TILDAS analyzer was positioned on the top right of the trailer, while the 2-D sonic anemometer and GPS unit were mounted on the top left of the trailer. (b) Driving track and measured NH_3 concentrations across the source area and the Veluwe forest area. The red arrow indicates the prevailing southwesterly wind direction during the drive. The background map is credited to Kadaster.nl.

https://doi.org/10.5194/egusphere-2026-2838
Preprint. Discussion started: 28 July 2026

2.3 Data processing and calibration

2.3.1 HT calibration

After the mobile campaign, HT measured NH_3 values were evaluated through field comparison with an independently operated mini Differential Optical Absorption Spectroscopy (mini-DOAS) 2.2D system at the Veenkampen site, in the Netherlands, using the similar set-up descripted by Swart et al., (2023). The comparison revealed that the HT measurements systematically underestimated NH_3 concentrations, likely due to calibration issues associated with the permeation tube used in the factory calibration unit. To correct for this bias, a non-linear transfer function was derived based on 2-month long co-located measurements under field conditions. This correction was applied to the HT data prior to further analysis.

Additional laboratory experiments were conducted after the campaign within the VSL Reference Gas Mixture (RGM) framework to characterize the response of the HT analyzer under controlled conditions, including the influence of temperature and humidity (Zhang et al., 2025). These experiments were performed using a different HT unit than that deployed during the 2023 campaign and were therefore not used to correct the field measurements. Instead, they provide supporting information on the general HT instrument response characteristics.

Data quality was ensured by excluding measurements with low optical signal strength (OSS < 10%) and by performing zero-drift checks before and after the mobile measurement period.

2.3.2 Plume definition and background removal

For this campaign, plumes were defined as Gaussian-shaped enhancements in gas concentration exceeding the instrumental noise by more than 1 ppb for both NH_3 and CH_4 measurements. However, natural variability in background concentrations was considered when selecting plumes. Only plumes with a peak concentration at least three times greater than the background variability observed within 5–10 seconds before and after the peak were selected. In practice, this corresponded to concentration enhancements in excess of ~5 ppb for NH_3 and ~10 ppb for CH_4. A second criterion required that each plume was traceable to a well-defined upwind source. Approximately three-quarters of the detected plumes met this criterion, with several sources confirmed by the operators. Potential sources were primarily identified using aerial imagery (Google Earth). For the remaining quarter, multiple potential sources were too close to each other to be individually resolvable and were therefore treated as multiple sub-sources in the plume modeling.

Although the Veluwe region contains many emission sources, the analysis focuses on short-lived concentration enhancements detected during mobile measurements rather than regional background levels. While NH_3 can be transported over long distances, dilution and overlap with emissions from multiple sources limit the detectability of individual plumes. However, near emission sources NH_3 concentrations may decrease due to dry deposition and gas–particle partitioning (Schulte et al., 2022; Yi et al., 2025), which may reduce plume contrast with distance and suppress the contribution of far away sources to transient enhancements.

Measurement distances were constrained by road accessibility for mobile sampling and therefore do not represent a detection limit. Under the conditions encountered during the campaign, clearly attributable plumes were typically observed at distances of ~50–800 m from the source. At larger separations, or when other emission sources were

https://doi.org/10.5194/egusphere-2026-2838
Preprint. Discussion started: 28 July 2026

present between the farm and the measurement location, plume attribution to a single source became ambiguous and such cases were excluded. Accordingly, the analysis focuses on well-defined near-road plumes associated with a single dominant source type.

Background concentrations were removed in two steps. First, the regional background was estimated by subtracting the 10th percentile within a 5-minute centered running mean window. Secondly, a plume-specific local background was removed by subtracting the minimum concentration observed across the plume period. The remaining signal was considered to represent plume enhancements, which were used for individual source emission analysis. Enhanced concentrations above background are expressed as ΔNH_3, ΔCH_4, and ΔCO.

2.4 Emission quantification methods

2.4.1 Integrated plume analysis and emission ratio approach

All plumes were subsequently integrated over time to obtain ΣNH_3 and ΣCH_4, representing the total gas enhancement of the plume, which is the amount of gas crossing the road at the measurement height of 3 m. The measured concentration reflects both the source strength and the dilution occurring between the source and the point of measurement, as described by Eq. (1):

$$C = S \times D \quad (1)$$

Where, C ($\mu g\ m^{-3}$) is the concentration measured at the transect, S ($g\ s^{-1}$) is the source strength, and D is the dispersion factor describing transport and dilution from the source to the measurement location, with units of (μg m^{-3}) / (g s^{-1}) or equivalently (s m^{-3}) after unit conversion.

For data interpretation, either the ratio of ΣNH_3 to ΣCH_4 was used, which largely cancels dilution effects, or the dilution was estimated using a Gaussian plume dispersion model (e.g. Hensen et al., 2009; Turner, 1994; Wietzel et al., 2025).

Source emission ratios between NH_3 and CH_4 can be determined using three approaches. First, the ratio of peak concentrations within the plume is simple but sensitive to noise and multiple peaks. Second, a linear regression of NH_3 versus CH_4 across the plume is less sensitive to instrument differences and small fluctuations. Third, the ratio of integrated concentrations (ΣNH_3 : ΣCH_4) provides the most representative estimate for complex plumes (Miller et al., 2015). In this study, the integrated-concentration approach was applied.

To minimize contamination from the measurement vehicle itself, data collected at low speeds or during turns (vehicle speed < 8 km h^{-1}) were excluded. The remaining data were used for on-road CO and NH_3 emission analyses (Zavala et al., 2009).

To distinguish traffic emissions from other local sources, we first applied the approach of Sun et al. (2014), identifying candidate traffic plumes based on enhanced CO (>100 ppb) and CO_2 (>15 ppm) after background removal. In the Veluwe region, however, some non-traffic sources (e.g. agricultural or waste-related emissions) also occasionally met these criteria. Therefore, additional screening was applied using CH_4 enhancements (>50 ppb) as an indicator of non-traffic influence. Plumes exceeding this CH_4 threshold were flagged and further

https://doi.org/10.5194/egusphere-2026-2838
Preprint. Discussion started: 28 July 2026

evaluated using wind direction, Google Earth imagery, and operator observations to ensure correct source attribution and to avoid mixing of multiple nearby sources.

2.4.2 Gaussian plume model

The observed plumes originating from various sources dispersed downwind, with both horizontal and vertical spreading approximating a Gaussian distribution. In this study, measured plumes were compared with plumes calculated using a Gaussian dispersion model as described by Vinković et al. (2022) and Hensen et al (2009).

Emission calculations were performed on a per-plume basis by comparing the integrated concentration patterns of measured and modeled plumes. The Gaussian plume model calculates positions along the plume axis perpendicular to it using wind direction, wind speed, stability class, source location, and the measurement vehicle's position. Dispersion parameters in the model are determined by the terrain roughness length (z_0) and the atmospheric stability class for the measurement episode. The stability class, following (Pasquill & Smith, 1983), indexes atmospheric turbulence and sets parameters that govern how rapidly the plume spreads with distance from the source.

Additional dispersion parameters include the characteristic travel time of air between the source and the measurement platform, typically on the order of 1–5 minutes. For the current dataset, measurement-day conditions were cloudy with wind speeds of approximately 2–4 m s^{-1}, corresponding to neutral to slightly unstable atmospheric conditions (Pasquill classes B or C). Roughness lengths were estimated for each source location based on land cover as identified from aerial imagery (Google Earth, December 2020, winter conditions) and manually verified using field notes and photographs taken during the February 2023 mobile campaign.

2.4.3 Agricultural emission inventory

For agricultural sources, NH_3 emissions depend on multiple factors, including management practices, mitigation technologies, animal feeds, and seasonal conditions (Gyldenkærne et al., 2005; Luo et al., 2025; Saha et al., 2014; Shan et al., 2025). To derive representative emission factors, repeated campaigns across the year are required. In contrast, traffic emissions are less sensitive to ambient conditions (Park et al., 2023; Wen et al., 2023), allowing the current campaign data to be used for on-road emission factor calculations. No specific agricultural activity data were available for the measurement period; therefore, inventory-based emissions were all downscaled to daily values, assuming negligible seasonal variations.

Livestock kept in animal housing represents a major source of NH_3 in the study area. Data on livestock farm characteristics, including housing type, animal numbers, emission height, and stable type, were obtained from the Dutch Core Registration of Animal Enclosures Database (Kernregistratie Dierverblijven, KRD) (Rijksdienst voor Ondernemend Nederland, n.d.-a). NH_3 emission factors per livestock house and per animal were applied based on Regeling ammoniak en veehouderij (RAV) guidelines (Rijksdienst voor Ondernemend Nederland, n.d.-b). CH_4 emission factors for cattle farms were derived from the RIVM National Inventory Report (NIR) (Van der Net et al., 2024), while default Intergovernmental Panel on Climate Change (IPCC) 2006 Tier 1 factors were used for swine and goats (IPCC, 2006). Poultry were excluded from the CH_4 emission factor analysis because their CH_4 emissions are negligible relative to other livestock.

https://doi.org/10.5194/egusphere-2026-2838
Preprint. Discussion started: 28 July 2026

Emissions from manured fields are highly variable, with peak emissions typically occurring within the first day after application. Although such sources were captured during the measurements, information on application rates and timing was not available. Therefore, these emissions are not suitable to directly compare with inventory values, and only their relative contribution on the measurement period is reported.

2.4.4 On-road emission factor derivation using a carbon balance approach

Traffic constitutes another significant source of NH_3, CO and CO_2 (EEA, 2025; Wang et al., 2023). For traffic sources, the method of Sun et al. (2014) was adapted to estimate on-road NH_3 emission factors using Eq. (2). While CO is a more specific tracer for vehicle emissions, CO_2 was used to quantify NH_3 emissions due to its dominant contribution to vehicular carbon by mole fraction. NH_3 emission factors (EF) are expressed in grams of NH_3 per kilogram of fuel burned, using a carbon balance approach.

$$EF = \left(\frac{\Delta NH_3}{\Delta CO_2 + \Delta CO}\right)\left(\frac{MW_{NH_3}}{MW_C}\right) W_C \quad (2)$$

where MW_{NH_3} and MW_C are the molecular weights of NH_3 (17 g mol^{-1}) and carbon (12 g mol^{-1}), respectively, and $W_C = 0.85$ represents the carbon mass fraction in gasoline. The carbon fraction for diesel ($W_C = 0.87$) was not included, as diesel vehicles have been shown to contribute only minimally to on-road NH_3 emissions (Burgard et al., 2006). ΔNH_3, ΔCO_2, and ΔCO represent the respective enhanced concentrations. Ratio calculations were restricted to peaks where ΔCO exceeded 100 ppb and ΔCO_2 exceeded 15 ppm, thresholds at which operators could clearly detect the passage of a vehicle and its associated plume.

2.5 Statistical analysis

Differences between independent source categories were statistically assessed using the Mann–Whitney pairwise U-test (Mann & Whitney, 1947) with $p < 0.05$ considered to indicate a significant difference. This nonparametric test is suitable for small sample sizes and non-normally distributed data and is particularly useful for comparing continuous data between groups with low numbers of observations.

To enable a robust comparison between measurement-based and inventory-based emissions for livestock farm sources, outliers (defined as large discrepancy values) were identified using the interquartile range (IQR) method, based on the ratio of measured to inventory-based emissions for both NH_3 and CH_4. The first (Q1) and third (Q3) quartiles were calculated, and the IQR was defined as Q3 − Q1. Values lying outside the range Q1 − 1.5 × IQR to Q3 + 1.5 × IQR were classified as outliers and excluded from subsequent analyses. After removal of these outliers, summary statistics (mean and median) were recalculated using the remaining data.

3 Results

3.1 Observed increments of NH_3, CH_4 and CO

On 21 February 2023, the mobile measurement covered approximately 160 km between 9:00 and 13:20 UTC around the Veluwe area. Calibrated NH_3 concentrations ranged from near zero to approximately 1300 ppb and exhibited strong spatial variability. Details of the HT calibration and validation are provided in the Supplement (Figs. S4 and S5). Due to the prevailing southwesterly wind, elevated NH_3 concentrations were observed in source-

https://doi.org/10.5194/egusphere-2026-2838
Preprint. Discussion started: 28 July 2026

intensified rural areas, particularly southwest and north of the Veluwe Natura 2000 site, while concentrations decreased sharply to near-background levels downwind in the northeast (Fig. 2b). Within the Veluwe nature reserve, NH_3 concentrations were typically below 3 ppb, whereas agricultural areas showed elevated baseline levels and frequent plume events (Fig. 2b).

Background-corrected time series of NH_3, CH_4, and CO illustrate plume signatures from four main source types: livestock housing, manured fields, a chemical waste treatment facility, and traffic (Figs. 3 and 4). NH_3 plume enhancements ranged from tens to hundreds of ppb, well above the detection limit, enabling robust identification of short-lived emission peaks. The strongest NH_3 enhancements were observed near a chemical waste treatment facility, followed by large livestock farms and manured fields (Fig. 4a). NH_3 and CH_4 plume enhancements remained detectable up to approximately 800 m downwind, depending on source strength. CH_4 concentration increased up to ~2 ppm above background level near agricultural sources, whereas in urban areas CO enhancements reached up to 2.5 ppm (Fig. 3).

Plume characteristics varied by source type. Livestock emissions showed co-enhanced NH_3 and CH_4 signals, reflecting their shared origin (Fig. 4b), while manured fields exhibited broader NH_3 plumes with comparatively weaker CH_4 enhancements (Fig. 4c). For more than 70% of the agricultural sources, NH_3 and CH_4 enhancements were moderately to strongly correlated ($R^2 > 0.71$), In contrast, traffic-related plumes were characterized by strong CO signals with lower NH_3 and CH_4 enhancements (Fig. 4d).

During the measurement period (~4.5 h), data coverage was ~90% for the HT analyzer (affected by short rain events) and 100% for the TILDAS. Zero-drift checks indicated stable baseline conditions, with no significant drift observed. In total, 49 sources were identified, with six livestock farms sampled twice, resulting in 55 plumes for further analysis. Of these, 41 originated from livestock farms (with either single or mixed animal types), seven from manured fields, three from long-lived traffic plumes (lasting > 5 s, sufficient for ΣNH_3:ΣCH_4 ratio calculations), and four from industrial sources. All plumes could be attributed to either individual sources or a cluster of nearby sources with modest to strong NH_3–CH_4 correlations. In addition, approximately 630 transient CO peaks coinciding with NH_3 enhancements were detected and attributed to passing vehicles (Fig. 3). These short-lived events were too brief for ΣNH_3:ΣCH_4 ratio calculations but were used to estimate NH_3 emission factors across driving speeds (Section 3.5).

https://doi.org/10.5194/egusphere-2026-2838
Preprint. Discussion started: 28 July 2026

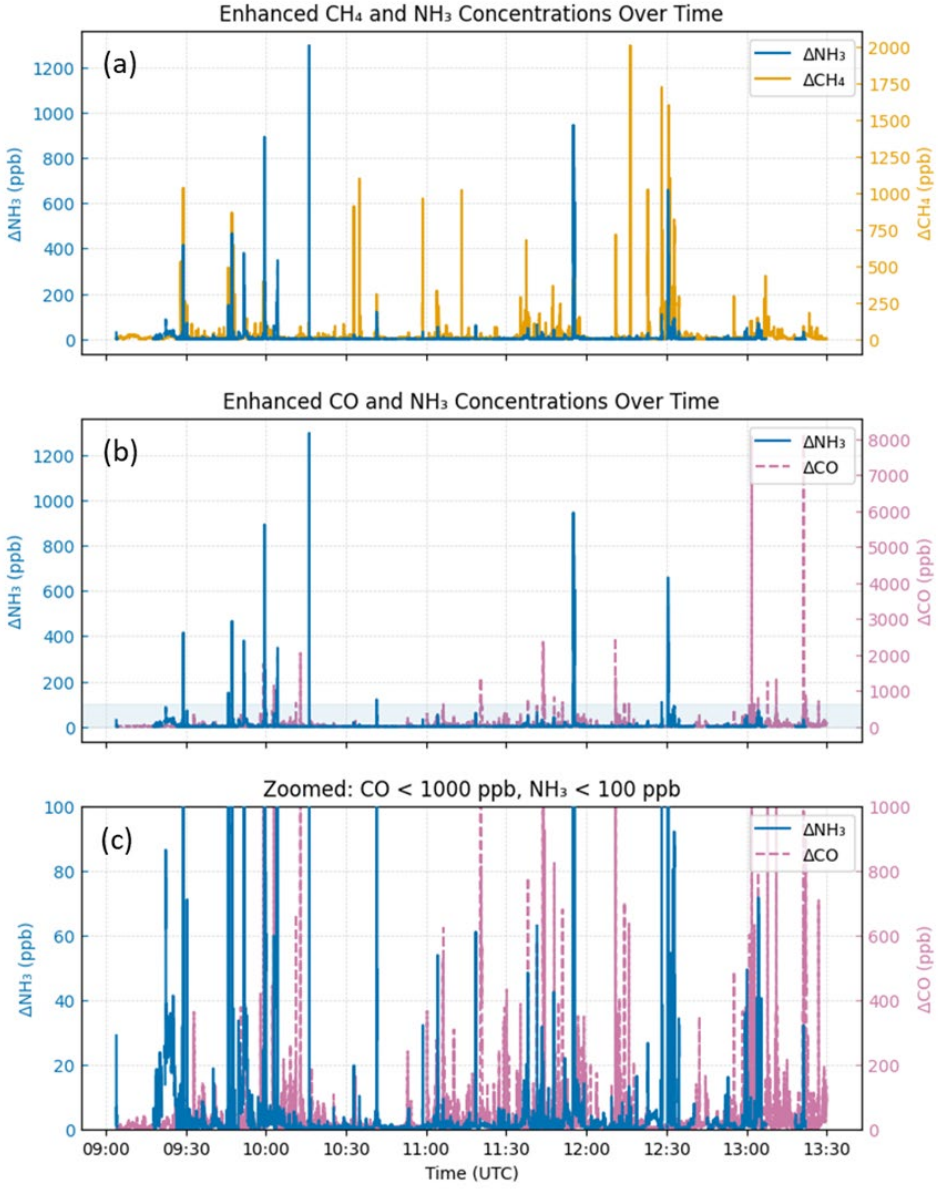

Figure 3: Time series (in UTC) of measured gas plumes after background removal: (a) NH_3 and CH_4, (b) NH_3 and CO, and (c) zoomed view of CO <1000 ppb and NH_3 <100 ppb for better visualization. In agricultural areas, CH_4 and NH_3 plumes overlap, whereas in (sub)urban areas, NH_3 and CO plumes overlap in the Veluwe region.

https://doi.org/10.5194/egusphere-2026-2838
Preprint. Discussion started: 28 July 2026

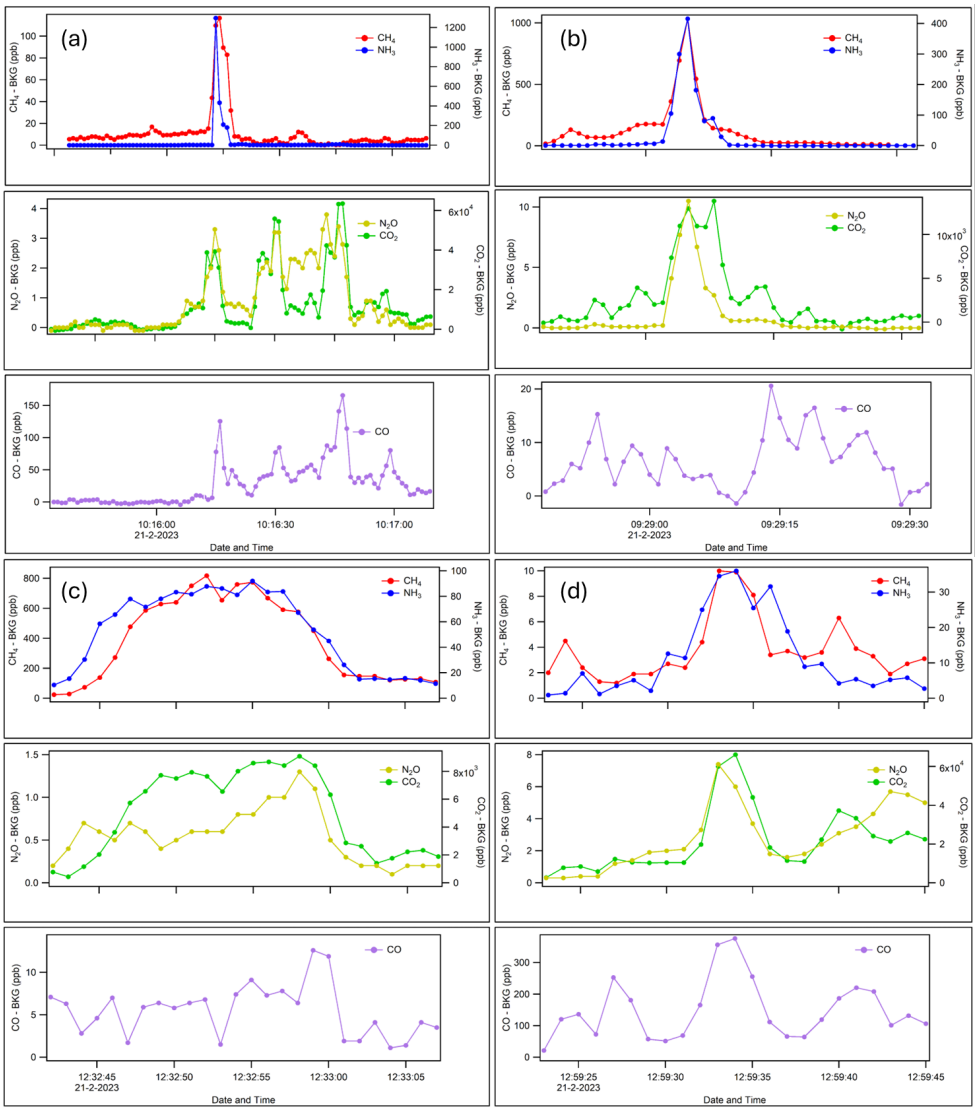

Figure 4: Examples of background-corrected concentrations of NH_3, CH_4, N_2O, CO_2, and CO measured at different source types: (a) a chemical waste treatment facility, (b) a cattle livestock farm, (c) a manured field, and (d) traffic sources.

3.2 ΣNH_3: ΣCH_4 ratios for agricultural emission sources

ΣNH_3:ΣCH_4 integral ratios provide a simple means to distinguish among agricultural source types. Among the 31 single species livestock farms (cattle, poultry, swine, or goat), ΣNH_3:ΣCH_4 ratios ranged from 0.01 to 1.1, with an overall median ± median absolute deviation (MAD) of 0.04 ± 0.02. Cattle and goat farms showed similarly low ratios (median ± MAD: 0.04 ± 0.06 and 0.04 ± 0.004, respectively), whereas swine and poultry farms exhibited substantially higher ratios (0.26 ± 0.02 and 0.42 ± 0.17, respectively). Manured fields displayed a median ratio of

https://doi.org/10.5194/egusphere-2026-2838
Preprint. Discussion started: 28 July 2026

2.1 ± 1.0, but spanned a wide range (0.84–8.1). This variability likely reflects differing emission dynamics, as CH_4 is primarily emitted during the first few hours following manure application, whereas ammonia emissions occur over a longer timescale of approximately two to four days after manure application (Sherman et al., 2022; Sommer et al., 2003). Mixed farms (n = 4), which contained multiple animal types, were excluded from the statistical analysis (Tables 1 and 2).

Figure 5 illustrates the variability in the ΣNH_3:ΣCH_4 ratios observed at all 31 single-species livestock farms across different measurement distances. The majority of cattle farms exhibited ΣNH_3:ΣCH_4 ratios of 0.05 or lower, although substantial variability was observed among individual farms. The limited number of observations from goat farms fell within a similar range. However, five cattle farms showed substantially higher ratios, with values reaching up to 0.42. These enhanced values were found occasionally, independent of distance to the source, which hints differences in farm-specific management practices or technologies, or contributions from manure storage emissions. Swine farms showed very little variation in the ΣNH_3:ΣCH_4 ratios, whereas the three poultry farms show ratio's far apart from each other.

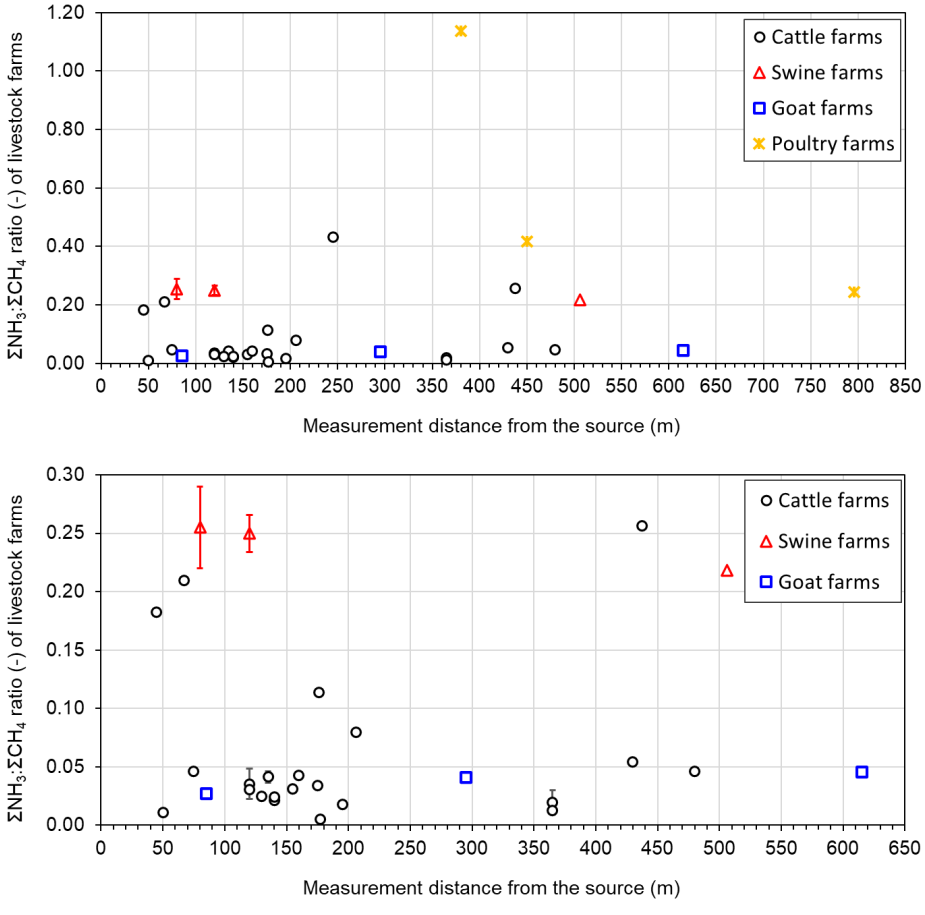

https://doi.org/10.5194/egusphere-2026-2838
Preprint. Discussion started: 28 July 2026

Figure 5: ΣNH₃:ΣCH₄ ratios for individual single-species farms plotted as a function of downwind distance (upper panel) to accessible driving roads for sampling. Distances reflect road accessibility, and data were excluded when other emission sources were present between the farm and the measurement location. A zoomed-in view highlighting the lower ratio range is shown in the lower panel. For farms sampled more than once during the day, the mean value and standard deviation are displayed.

3.3 Inversion results compared to emission estimates for livestock farms

The ΣNH₃:ΣCH₄ ratio shows promise to disentangle different agricultural source types but for a quantitative emission estimation one needs to perform an inverse model approach. To enable an indicative comparison between the mobile-based measurements and inventory-derived emissions, Gaussian plume modelling was applied to estimate CH_4 and NH_3 emissions for the livestock sources with available inventory data (Fig. 6, Fig. S2 and Table S1 in the Supplement). The model accounted for source type, wind speed and direction, and terrain roughness (z_0) for each plume.

Among the livestock plumes, six sources were measured twice within the same day. The resulting variability, expressed as the coefficient of variation (CV), was generally lower for CH_4 (2–30%) than for NH_3 (4–59%), indicating greater short-term variability in NH_3 emissions.

Annual inventory data (animal type and numbers from KRD) were available for 25 NH_3 sources and 22 CH_4 sources that were measured in the day (Fig. 6, Table S1). Discrepancies between measurement-based and inventory-based emissions were larger for NH_3 than for CH_4 when expressed as emission ratios (modelled / inventory; mean ± SD: 3.5 ± 5.4 versus 3.1 ± 5.0). Using the interquartile range (IQR) method, two high-end NH_3 values and two CH_4 values were identified as outliers and excluded to reduce the influence of extreme values on summary statistics. The remaining NH_3 ratios yielded a mean ± SD of 2.2 ± 2.2 and a median of 1.4, while CH_4 showed 1.8 ± 1.2 and a median of 1.7. Furthermore, CH_4 emissions exhibited a moderate correlation between inventory-based and measurement-based estimates ($r \approx 0.66$), whereas NH_3 showed only weak agreement ($r \approx 0.37$). This indicates substantially larger discrepancies for NH_3 compared to CH_4 (Fig. S3 in the Supplement).

Inventory-measurement discrepancies seems also depend on animal type. Using modelled / inventory ratios, cattle farms exhibited the closest agreement (NH_3 median = 1.1, CH_4 median = 1.5; n = 13), higher NH_3 ratios for swine (median = 6.1; n = 3) and mixed-species farms (median = 5.6; n = 4), intermediate discrepancies for poultry (NH_3 median = 2.2; n = 3). CH_4 ratios were generally smaller and less variable across animal types (median range ≈ 1.4–3.2; poultry excluded due to missing CH_4 inventories) (Fig. 6).

https://doi.org/10.5194/egusphere-2026-2838
Preprint. Discussion started: 28 July 2026

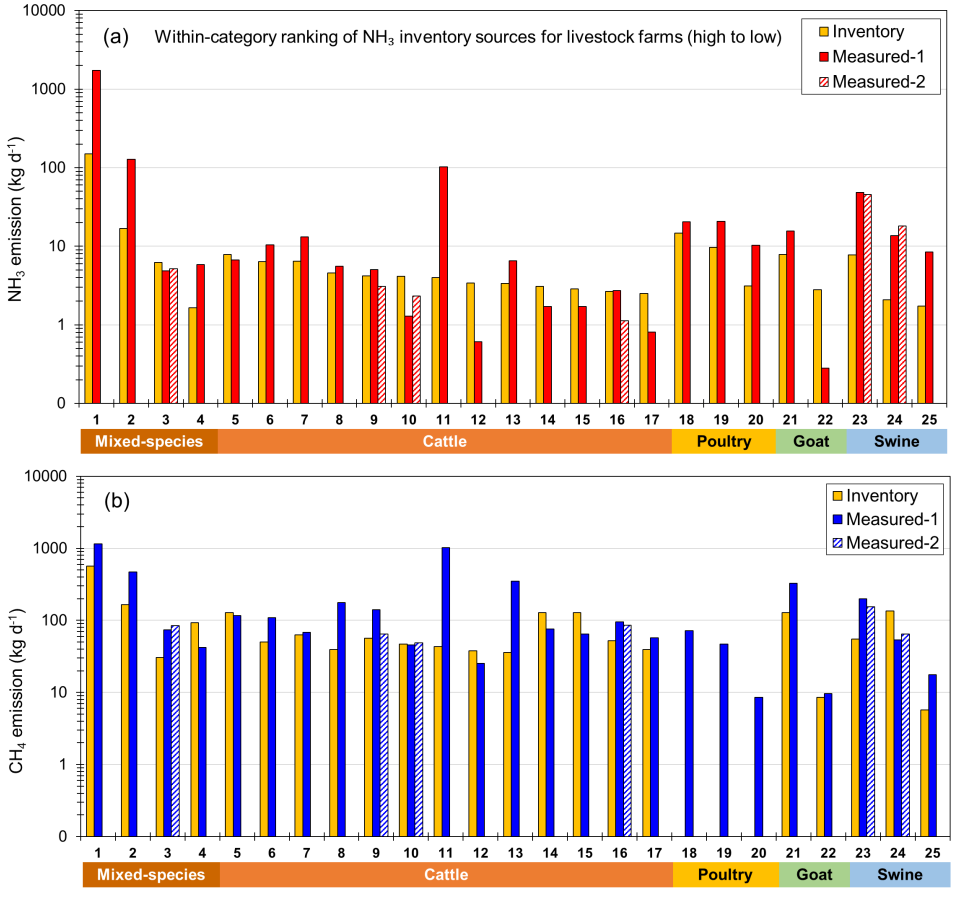

Figure 6: Comparison of measured NH_3 emissions (Gaussian plume inference) with KRD inventory-reported values for cattle, poultry, swine, and mixed-species livestock farms. Data are shown on a logarithmic scale and ordered by NH_3 inventory emissions per category (upper panel). The lower panel presents the corresponding CH_4 comparison using the same NH_3-based ranking. Farms measured once (measured-1) and twice (measured-2) are indicated in the legend. Only sources with available inventory data are shown.

3.4 Comparison with non-agricultural sources

Plumes from non-agricultural sources were evaluated to determine whether they could be distinguished from agricultural plumes using the ΣNH_3:ΣCH_4 ratio. Among livestock farms, cattle and goat farms exhibited low ratios (median ± MAD: 0.04 ± 0.02 and 0.04 ± 0.00, respectively), which were significantly lower than those observed for swine and poultry farms (0.25 ± 0.01 and 0.42 ± 0.17, respectively; $p < 0.05$, Table 2), reflecting differences in emission dynamics among animal types.

Manured fields showed substantially higher ratios (2.11 ± 1.03) than livestock sources ($p < 0.05$), consistent with enhanced NH_3 emissions relative to CH_4 following manure application. The three long-lived traffic plumes

https://doi.org/10.5194/egusphere-2026-2838
Preprint. Discussion started: 28 July 2026

observed during the campaign exhibited markedly elevated ΣNH_3:ΣCH_4 ratios (4.59 ± 0.34), clearly exceeding those of livestock farms, manured fields, and most industrial sources. Pairwise Mann–Whitney U tests indicate that traffic plumes are significantly different from livestock sources ($p < 0.01$), while differences relative to industrial sources were not statistically significant, reflecting partial overlap and limited sample size (Table 2).

Industrial sources, including an agricultural service company, a chemical waste treatment facility, and two logistics sites, displayed intermediate but variable ratios (0.47 ± 0.37; range 0.06–2.10), indicating heterogeneous emission characteristics. Statistical tests show that industrial ratios overlap with both livestock and manured-field emissions, whereas the highest ratios remain characteristic of traffic plumes (Tables 1–2; Fig. 7).

Despite the use of robust summary statistics (median and MAD), some manure-related ratios overlap with industrial or traffic sources, highlighting the limitations of using ΣNH_3:ΣCH_4 ratios alone for source discrimination. The small number of traffic and industrial observations further constrains statistical power, and results should therefore be interpreted with caution. Nonetheless, the observed contrasts indicate that ΣNH_3:ΣCH_4 ratios provide useful, first-order discrimination between traffic and most agricultural sources, particularly when interpreted in conjunction with contextual information. Sampling of non-agricultural sources outside manure-application periods is advisable, as temporal overlap may otherwise complicate source attribution.

https://doi.org/10.5194/egusphere-2026-2838
Preprint. Discussion started: 28 July 2026

Table 1: Statistical overview (median ± MAD) of different source categories, showing the ΣNH_3:ΣCH_4 ratio ranges for the captured sources during the 21 February 2023 Veluwe campaign. Note: Only three traffic plumes met criteria for NH_3:CH_4 ratio calculation. The other transient traffic-related peaks were not included in this analysis (see text).

Source category	Subtype	n	ΣNH_3:ΣCH_4 (Median ± MAD)	Range
Livestock farms		31	0.04 ± 0.02	0.01 - 1.14
	Cattle	22	0.04 ± 0.02	0.01 - 0.43
	Goat	3	0.04 ± 0.004	0.03 – 0.05
	Swine	3	0.25 ± 0.01	0.22 - 0.26
	Poultry	3	0.42 ± 0.17	0.24 - 1.14
Manured fields	—	7	2.11 ± 1.03	0.84 - 8.14
Traffic sources	—	3	4.59 ± 0.34	2.99 - 4.92
Industrial sources	—	4	0.47 ± 0.37	0.06 - 2.10

Table 2: Mann-Whitney pairwise test p-value results among different source categories. Results with $p < 0.05$ are indicated in bold italic font with a star sign (*) to highlight significant differences between sources.

Source type (sample number)	Cattle (22)	Goat (3)	Swine (3)	Poultry (3)	Manured field (7)	Traffic (3)	Industry (4)
Cattle (22)	—	0.969	***0.006****	***0.003****	***1.0×10⁻⁶****	***0.001****	***0.010****
Goat (3)	0.969	—	0.100	0.100	***0.017****	0.1	0.057
Swine (3)	***0.006****	0.100	—	0.400	***0.017****	0.1	1.000
Poultry (3)	***0.003****	0.100	0.4	—	***0.033****	0.1	0.857
Manured fields (7)	***1.0×10⁻⁶****	***0.017****	***0.017****	***0.033****	—	0.517	***0.042****
Traffic (3)	***0.001****	0.100	0.100	0.100	0.517	—	0.057
Industry (4)	***0.010****	0.057	1.000	0.857	***0.042****	0.057	—

https://doi.org/10.5194/egusphere-2026-2838
Preprint. Discussion started: 28 July 2026

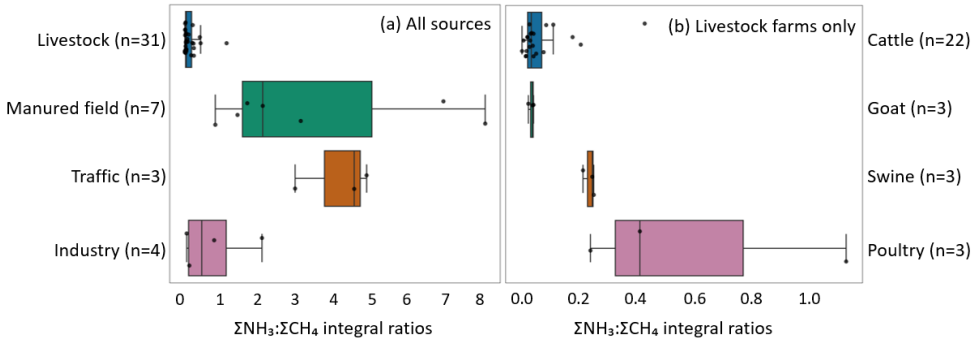

414

415 **Figure 7: Boxplots of ΣNH₃:ΣCH₄ integral ratios for different source categories. (a) Comparison of four major source**
416 **types: livestock farms, manured fields, traffic, and other, industry-related sources. (b) Variation in ΣNH₃:ΣCH₄ ratios**
417 **among livestock subcategories (cattle, poultry, swine, and goats). The central line represents the median value; box**
418 **edges denote the 25th and 75th percentiles; whiskers extend to the 5th and 95th percentiles; and solid black dots indicate**
419 **outliers.**

https://doi.org/10.5194/egusphere-2026-2838
Preprint. Discussion started: 28 July 2026

3.5 Traffic emission factors and comparison with national inventory

On-road traffic emits CO, CO_2, and NH_3, with NH_3 produced mainly by vehicles equipped with three-way catalytic converters. As stated previously, the ~630 transient CO peaks identified along the drive were too brief to allow ΣNH_3:ΣCH_4 ratio calculations but they provided a sufficiently large dataset for estimating NH_3 emission factors (EFs) across driving speeds (Figs. S2 and S3).

The median NH_3-to-carbon EF value was 0.18 g kg^{-1}, consistent with the geometric mean of 0.18 g kg^{-1} (Table 3). NH_3 EFs showed a positive association with driving speed. On highways (≥80 km h^{-1}), EFs were significantly higher than those in urban traffic conditions (20–80 km h^{-1}). At very low speeds (8–20 km h^{-1}), typically corresponding to vehicle turns, traffic jams, traffic lights, or roundabouts, the NH_3 EF was markedly reduced (Table 3). Vehicle class immediately ahead was not recorded for individual plume encounters. Figure 8b illustrates the corresponding EF distributions per speed category whereas the related traffic source peaks under different road types are shown in Fig. 8a and Fig. S1.

For comparison, the 2023 Netherlands traffic emission inventory reported by CBS indicates total motor vehicle emissions of 27.1 Mt CO_2, 163.6 kt CO, and 3.8 kt NH_3, corresponding to an NH_3-to-carbon ratio of approximately 0.14 g kg^{-1}. Measurement-derived NH_3 EFs for low-speed traffic conditions (< 60 km h^{-1}) were within the same range as this inventory-based ratio, whereas higher EFs were observed for traffic speeds exceeding 60 km h^{-1}.

Table 3: Traffic speeds and related geometric means (and standard deviations) per speed category of the NH_3 emission factor (EF in g NH_3 / kg fuel) using the carbon balance approach.

	8-20 km h^{-1}	20-60 km h^{-1}	60-80 km h^{-1}	≥ 80 km h^{-1}	All > 8 km h^{-1}
Number of samples	76	306	150	95	627
Geometric mean	0.12	0.16	0.19	0.28	0.18
Geometric SD	3.19	2.68	2.16	1.76	2.55
Median	0.10	0.16	0.20	0.31	0.18
Q_{25}	0.05	0.08	0.11	0.19	0.09
Q_{75}	0.24	0.25	0.35	0.41	0.32
Min.	0.01	0.02	0.04	0.04	0.01
Max.	6.9	19	0.85	0.88	19

https://doi.org/10.5194/egusphere-2026-2838
Preprint. Discussion started: 28 July 2026

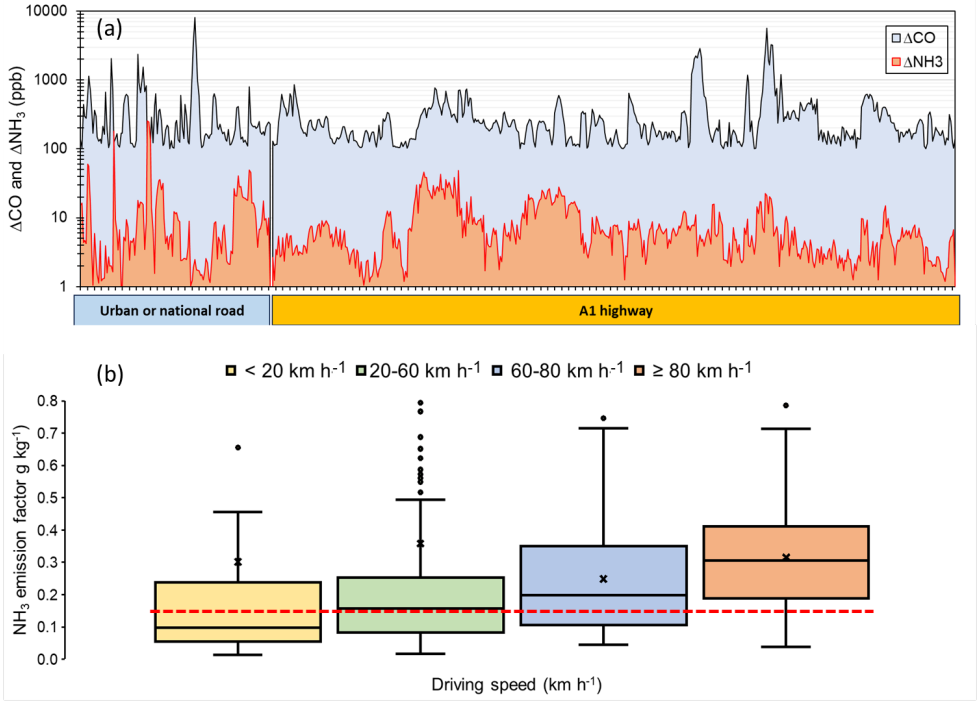

Figure 8: (a) Time-series of traffic-related NH_3 (orange) and CO (blue) concentration enhancements during urban and highway driving (logarithmic scale). (b) Boxplots of NH_3 emission factors as a function of driving speed, illustrating their dependence on traffic conditions. The red dash line indicates the average EF value based on the 2023 Netherlands traffic emission inventory (0.14 g kg^{-1}).

4 Discussion

The objective of this study was to demonstrate the use of a mobile measurement platform to characterize real-world ammonia emission sources in the vicinity of the Veluwe Natura 2000 area, capturing both observed concentrations and inferred emission characteristics. During a half-day mobile measurement campaign, an area of approximately 1,500 km^2 was surveyed, yielding plume-based emission information for 49 individual, well-defined sources. By simultaneously measuring NH_3, CH_4, and CO, we were able to distinguish agricultural and traffic-related emissions and to assess source-specific emission ratios under real-world conditions. Although the region surrounding the Veluwe contains a large number of potential NH_3 emitters, only sources located relatively close to the measurement route and aligned with prevailing wind conditions provided well-defined Gaussian-shaped plumes required for source characterization. Contributions from more distant sources are therefore expected to manifest primarily as background variability and do not materially influence the plume-based emission ratios derived here. Within this framework, the selection of sources provided a first insight into important agricultural emission and into both local and regional traffic emission characteristics relevant to the Veluwe area.

https://doi.org/10.5194/egusphere-2026-2838
Preprint. Discussion started: 28 July 2026

The open-path configuration of the NH_3 analyzer, combined with high measurement frequency, allowed for the effective capture of both on-road and downwind NH_3 emissions with minimal signal damping, an advantage not achievable with closed-path instruments (Lemes et al., 2023; Miller et al., 2015). Moreover, the applied method not only enabled detection of traffic- and agricultural emissions, but also holds potential for identifying and characterizing emissions from large industrial sources, such as chemical waste treatment facilities (Table S1 and Fig. S2 in the Supplement).

4.1 Application of the ratio method and its limitation

The enhanced concentration ratio method (ΣNH_3:ΣCH_4) was applied to quantify emissions from different agricultural source types. For more than 70% of the agricultural sources, NH_3 and CH_4 enhancements were moderately to strongly correlated ($R^2 > 0.71$), indicating that both species originated from a common source and that plume dilution effects were largely consistent across the measurement transect. This supports the applicability of integrated concentration ratios for source characterization under mobile sampling conditions.

As expected, ruminant animals (such as cattle and goats) exhibited much lower ΣNH_3:ΣCH_4 ratios compared to non-ruminant animals (such as poultry and swine) (Table 1, Fig. 7). This outcome reflects fundamental physiological and management differences: ruminant enteric fermentation produces large CH_4 emissions relative to NH_3 (Liu et al., 2017), and direct field measurements show that dairy cattle manure emits over five times more CH_4 than swine manure (Zhuang et al., 2020). Livestock emission inventories further indicate that cattle often dominate total NH_3 emissions while also generating substantial enteric CH_4, thereby lowering the NH_3:CH_4 ratio relative to monogastric animals (Jiang et al., 2024). These distinct ΣNH_3:ΣCH_4 ratios can help constrain the dominant livestock type in barns to some extend, but the observed within-type variability and overlap indicate that the ratio is most robust as a supporting indicator rather than a definitive separator. In regions with comprehensive agricultural statistics, such information may be readily available, but in many parts of Europe and worldwide, data on the precise locations of housing emissions are often incomplete or not publicly accessible. Hence, the ratio method provides a valuable approach for inferring livestock sources where official spatial emission data are limited.

This study represents the first regional mobile deployment in the Europe combining HT-based open-path NH_3 measurements with TILDAS-based greenhouse gas observations. While the dataset provides valuable first-order insights, such as clear differentiation between livestock types, manured fields, traffic, and industrial sources, the limited temporal coverage restricts assessment of diurnal, seasonal, and meteorological variability. Multiple campaigns spanning different seasons and time-of-day conditions will therefore be required to improve statistical robustness and to better constrain variability in NH_3 and CH_4 emission across source types.

4.2 Drivers of Spatial Variability in ΣNH_3:ΣCH_4 Ratios

Near-source concentration declines are driven primarily by strong atmospheric dilution, which affects both NH_3 and CH_4 in similar manner (Miller et al., 2015; Nair & Yu, 2020). Consistent with previous studies, we also observe an exponential decrease in plume enhancements above background levels with increasing distance from the source. Despite this rapid dilution, mobile measurements enabled source identification at distances of up to 800 m from the road, which is notable given the high density of livestock farms in the study area.

https://doi.org/10.5194/egusphere-2026-2838
Preprint. Discussion started: 28 July 2026

Our results reveal substantial variability in ΣNH_3:ΣCH_4 ratio across livestock types and individual farms in pasture-dominated landscapes. In particular, individual cattle farms exhibit pronounced heterogeneity in ΣNH_3:ΣCH_4 ratios. This heterogeneity may be explained by site-specific conditions, such as farming practice, housing and or manure storage type or simply the age of the animals or the (variable) number of animals (Lichtfouse, 2012; McCabe et al., 2023; Yang et al., 2022). Variations in animal numbers may be especially relevant for calf-rearing farms and poultry (broiler) farms, where population sizes can fluctuate markedly over short timescales (Ruyssenaars et al., 2020; Van der Net et al., 2024).

Note that the processes responsible for the ammonia emission are distinctly different than those for methane. Methane emissions depend primarily on enteric fermentation and feed management strategies (Liu et al., 2021). Ammonia emissions intrinsically depend on the evaporation of ammonia from Total Ammoniacal Nitrogen (TAN) pools (Jiang et al., 2024). The latter means that ammonia emissions, in contrast to methane, are highly dependent on meteorology, with much larger emissions at high ambient temperature than at low temperature (Gyldenkærne et al., 2005). Hence, the ΣNH_3:ΣCH_4 are anticipated to vary with season and synoptic situation. Moreover, whereas the ammonia emission may vary over the day as function of temperature, the methane emissions vary with feeding practice (Saha et al., 2014) leading to variable ΣNH_3:ΣCH_4 ratios throughout a day. Although these aspects may not be important for the current single day proof of concept study, it means that measurements in different meteorological conditions are required to obtain a good grip on the fingerprinting and emission quantification process based on mobile measurements.

In theory, the ΣNH_3:ΣCH_4 is expected to decline systematically over distance due to the removal of ammonia through dry deposition (Asman et al., 1998; Flechard et al., 2011). Near-source deposition (within ~1 km) may remove a fraction of total NH_3 emissions, typically in the order of 5–10%. For example, ~8% of annual NH_3–N was estimated to be deposited within 1 km of an Australian feedlot (Shen et al., 2016), 5–10% within 1 km for a poultry farm (Fowler et al., 1998), and ~10% of NH_3 dry deposition occurred within 500 m of a swine production site in United States (Miller et al., 2015; Nair & Yu, 2020). The magnitude of NH_3 loss due to near-source dry deposition is substantially smaller than the variability observed in ΣNH_3:ΣCH_4 ratios among individual farms in this study (Fig. 5). Consequently, our measurements do not allow any conclusions regarding the influence of near-source dry deposition on the observed ratios. Future work could address this process through repeated, high-resolution measurements downwind of individual farms, including transects driven parallel to the wind direction to quantify systematic changes in ΣNH_3:ΣCH_4 ratios within a single plume.

Overall, these findings demonstrate that ΣNH_3:ΣCH_4 ratios are highly dynamic with livestock type, and management practices, whereas CH_4 remains a comparatively robust spatial tracer. Accurate assessment of agricultural NH_3 emissions therefore requires integrated NH_3–CH_4 measurements combined with deposition-aware interpretation, particularly in heterogeneous agricultural landscapes.

4.3 Uncertainty of on-road mobile measurements for NH_3 emission estimation

When all available farm sources were ranked, approximately 60% of the scanned livestock sources exhibited emission estimates exceeding the annual inventory-based values for both NH_3 and CH_4 (Fig. 6). After excluding

https://doi.org/10.5194/egusphere-2026-2838
Preprint. Discussion started: 28 July 2026

outliers, the mean ratio between measurement-based and inventory-based emissions was larger for NH_3 than for CH_4 (2.2 ± 2.2 versus 1.8 ± 1.2), indicating a systematically greater discrepancy for NH_3. The predominance of measurement-based estimates exceeding inventory values suggests that inventories may underestimate emissions under certain conditions; however, contributions from measurement uncertainties and short-term emission peaks cannot be excluded. This pattern is consistent with earlier satellite-based and ground-based studies reporting larger uncertainties and deviations for NH_3 compared to more stable tracers such as CH_4 (Shen et al., 2016; Van Der Graaf et al., 2022).

The larger discrepancies observed for NH_3 likely reflect its strong sensitivity to meteorological and surface conditions, including temperature, humidity, and boundary-layer dynamics (Asman et al., 1998; Flechard et al., 2011), as well as its dependence on short-term agricultural management activities such as manure handling and field application. In contrast to CH_4, NH_3 emissions can vary substantially on short time scales, causing short-lived concentration enhancements that may exceed temporally averaged inventory estimates based on annual emission factors (Velthof et al., 2012). The open-path measurement approach minimizes instrumental artefacts such as inlet adsorption and delayed response, suggesting that much of the observed variability reflects real atmospheric and emission variability rather than measurement bias.

An additional source of uncertainty arises from the field calibration applied to the HT NH_3 measurements. The calibration function was derived from co-located miniDOAS observations under ambient and moderately enhanced conditions (~1–100 µg m^{-3}), whereas substantially higher concentrations were occasionally encountered during mobile plume measurements. Consequently, the concentration correction was partly applied outside the primary calibration range, which may introduce additional uncertainty at the highest observed NH_3 concentrations. Nevertheless, the calibration substantially improved agreement between the HT and independently operated miniDOAS observations and primarily affected the absolute magnitude of NH_3 enhancements rather than the spatial occurrence of plumes or the relative differences between source types. Therefore, calibration-related uncertainty is not expected to alter the main conclusions regarding the spatial variability and relative magnitude of NH_3 emissions observed during the campaign.

Differences between measured and inventory-based NH_3 and CH_4 emissions further reflect variability in agricultural practices. Emissions from poultry farms, manure application, and grazing are highly variable in time and space and contribute substantially to inventory uncertainty. For example, manure-related field emissions have been estimated to contribute up to 37% uncertainty at fine spatial scales, while grazing contributes up to 49% at broader scales (Lessmann et al., 2025). Such temporally dynamic activities are known to explain a substantial fraction of discrepancies between bottom-up inventories and measurement-based estimates (Lessmann et al., 2025; Van Der Graaf et al., 2022).

More accurate quantification of individual emission sources using mobile plume measurements generally requires multiple downwind transects (typically 6–10) to reduce uncertainty (Maazallahi, 2022; Tettenborn et al., 2025; Wietzel et al., 2025). In this study, only one or two transects per source were recorded, resulting in substantial uncertainty for individual emission estimates. Additional uncertainty arises from assumptions in the Gaussian plume model, including steady-state conditions, homogeneous turbulence, and uncertainties in wind fields and

https://doi.org/10.5194/egusphere-2026-2838
Preprint. Discussion started: 28 July 2026

plume interception during mobile sampling. However, the primary objective was not precise quantification of single sources in a single measurement pass, but rather to demonstrate the feasibility of mobile NH_3 measurements and to compare emission characteristics across an ensemble of sites. Future studies should focus on optimizing measurement strategies to derive more accurate emission estimates for highly variable ammonia sources.

In addition to quantifying emissions, the mobile measurements also revealed several previously unregistered sources, particularly near provincial boundaries (e.g. between Gelderland and Overijssel; Table S1, Fig. S2 in the Supplement), highlighting the method's potential for identifying overlooked or misclassified sources. Similar inventory gaps have been documented in other sectors, where a significant fraction of emitting sources were absent from bottom-up records (Jiang et al., 2024; Vogel et al., 2024).

Overall, despite limited temporal coverage, mobile measurements provide high spatial resolution and near-source sensitivity (Maazallahi, 2022), offering a valuable complement to inventory-based and remote-sensing approaches for characterizing heterogeneous and temporally variable NH_3 emissions.

4.4 Estimated NH_3 traffic emission factors from on-road measurement data

In our study, the NH_3-to-carbon ratio indicated that traffic-related NH_3 emissions contributed substantially less to the regional atmospheric NH_3 enhancements than agricultural sources during the measurement period as expected (Table 2, Fig. 1). The derived geometric mean on-road traffic NH_3 emission factor of 0.18 g kg^{-1} (geometric SD = 2.55) for the relatively sparsely populated Veluwe area is substantially lower than values reported for major urban regions such as Beijing and California (Sun et al., 2017), and also below the mean value of 0.44 g kg^{-1} derived from traffic-related measurements across multiple urban environments (Pu et al., 2023). These results highlight the dominant role of agricultural emissions in shaping local NH_3 concentrations and suggesting that mitigation efforts in the region should prioritize agricultural emissions.

In a broader context, several studies have shown that vehicle-related NH_3 emissions are frequently underestimated in emission inventories, particularly in urban environments. For example, urban passenger car NH_3 emissions in the UK were found to be underestimated by a factor of 17 (Farren et al., 2020), while Dutch studies identified both three-way catalytic converters and SCR-equipped heavy-duty vehicles as important NH_3 sources not adequately captured by COPERT-based emission factors (Stelwagen & Ligterink, 2015).

Within this context, our measurements show a clear dependence of NH_3 emission factors on driving speed. Highway traffic conditions were associated with higher NH_3 emission factors (0.28 g kg^{-1}; Table 3) than urban driving conditions (0.19 g kg^{-1}), with both exceeding the NH_3-to-carbon ratio implied by the National Emission Inventory (0.14 g kg^{-1}; CBS, 2023). This suggests that emissions under high-speed or high-load conditions may be insufficiently represented in current inventories. Although our observations are limited in spatial and temporal coverage, they indicate potentially important contributions from highway traffic that warrant further investigation.

Previous studies have reported a U-shaped relationship between vehicle speed and NH_3 emissions, with maxima at low and high speeds and minima at moderate cruising speeds (Kean et al., 2009; Li et al., 2021). In contrast, our results indicate a more monotonic increase with speed (Fig. 8b), likely reflecting limited sampling of low-speed,

https://doi.org/10.5194/egusphere-2026-2838
Preprint. Discussion started: 28 July 2026

stop-and-go traffic. More generally, recent work highlights that NH_3 formation depends on a combination of driving dynamics, engine load, and after-treatment performance rather than speed alone (Farren et al., 2020; Jiang et al., 2023; Wen et al., 2025). These findings highlight the importance of accounting for driving behavior, fleet composition, and emission control technologies (Brinklow et al., 2023; Li et al., 2021) when interpreting speed-dependent NH_3 emission factors and translating localized measurements to inventory-scale assessments.

For traffic-related emissions, uncertainties arise from the lack of vehicle-specific, speed-resolved data, as differences in fleet composition and driving conditions likely influence observed emission patterns. Nevertheless, the mobile observations successfully captured on-road NH_3 plumes and revealed systematic changes in NH_3 to carbon enhancement ratios with vehicle speed (Fig. 8b and Fig. S1), demonstrating the capability of the approach to detect real-time traffic-related NH_3 emissions.

5 Conclusions

A mobile measurement platform equipped with an open-path HT-8700E NH_3 analyzer and a closed-path Aerodyne TILDAS QCL-based multi-gas analyzer was deployed during a mobile drive in the Veluwe area (central Netherlands) on 21 February 2023 to demonstrate its capability to characterize and quantify ammonia emission sources along a 160 km route. Multiple emission plumes containing NH_3, CH_4, and CO were detected from a range of agricultural and non-agricultural sources. Several previously unregistered sources were also identified, highlighting potential gaps in existing emission inventories. Plume-integrated enhancement ratios (ΣNH_3:ΣCH_4) were evaluated across 49 distinct sources, and source-specific CH_4 and NH_3 emission rates were estimated using an inverse Gaussian plume dispersion model and compared with the 2023 national livestock emission inventory.

This study demonstrates that the concentration ratio ΣNH_3:ΣCH_4 derived from mobile measurements provides a useful metric for identifying and characterizing emission source types in heterogeneous agricultural landscapes. Livestock farms exhibited characteristically low ratios, with median values of 0.04 for cattle and goat farms, 0.26 for swine farms, and 0.42 for poultry farms, reflecting fundamental differences in emission processes. In contrast, traffic emissions showed much higher ratios (median 4.6), while manured fields displayed intermediate and highly variable ratios (median 2.1, range 0.84–8.1), consistent with temporally variable NH_3 and CH_4 release following manure application. These contrasting signatures demonstrate the potential of combined NH_3 and CH_4 observations for source attribution during mobile monitoring campaigns, although partial overlap between source-specific ratios limits strict source separation.

Emission estimates derived from plume inversion showed closer agreement with inventory values for CH_4 than for NH_3. The larger discrepancies observed for NH_3 likely reflect its stronger sensitivity to meteorological conditions, short-term agricultural activities, and uncertainties associated with highly dynamic near-source emission and NH_3 deposition. In addition, uncertainties related to plume sampling strategy, atmospheric variability, limited temporal sampling, and calibration outside the primary concentration range may contribute to the spread in individual NH_3 emission estimates. Nevertheless, the observed spatial patterns and relative differences between source categories remained robust.

https://doi.org/10.5194/egusphere-2026-2838
Preprint. Discussion started: 28 July 2026

In urban areas and along highways, traffic-related NH_3 emissions were clearly detectable together with CO and CO_2, demonstrating the capacity of the mobile platform to characterize combustion-related NH_3 sources under real-world driving conditions. Measured NH_3 emission factors showed substantial variability with driving speed and exceeded inventory-based values under highway conditions, indicating that traffic-related NH_3 emissions may be more variable than represented in current inventories. Future integration with vehicle identification approaches could further improve attribution of traffic-related emissions to specific vehicle classes and emission-control technologies.

Overall, simultaneous mobile measurements of NH_3 and greenhouse gases provide an efficient approach for mapping and characterizing multiple emission sources over short time periods. The robustness and representativeness of such datasets can be further improved through repeated measurements across seasons, times of day, and meteorological conditions, enabling better characterization of emission variability across both agricultural and urban environments.

Code and data availability

The data underlying this study, including those used to generate the figures and the analysis code, are available from the authors upon request. Detailed Global Positioning System (GPS) coordinates are not publicly shared in order to protect the privacy of individual farmers and to prevent direct linkage between specific locations and measured emissions.

Authors contributions

AH, PvdB and MS co-designed the experiments and driving rout. PvdB, DvD, and JZ conducted the field measurements and data collection. JZ, AH and BT developed the model code and performed the Gaussian plume simulations. IV and GJdB merged the raw mobile measurement data and carried out the initial data screening. JZ, BT, and GJdB conducted figure preparation and spatiotemporal analysis. JZ, BT, and ED performed the source investigation, inventory data search, and analysis. JZ and AH prepared the original manuscript, with contributions from all co-authors through discussion and editing. MS, AH, and PB acquired the funding.

Competing interests

The authors declare that they have no conflict of interest.

Acknowledgement

We gratefully acknowledge the financial support from the Netherlands Ruisdael Project, the Dutch Ministries of Infrastructure & Water Management, and Agriculture, Nature & Food Quality as well as the TNO KIP project for

https://doi.org/10.5194/egusphere-2026-2838
Preprint. Discussion started: 28 July 2026

Nitrogen Research. We thank our TNO colleague Pascal Wintjen and Sampurno Bruijnzeel of King's College London for their valuable comments. Finally, we acknowledge Harmen van Mansom for preparing and inspecting the HT instrument prior to the mobile measurement campaign. Finally, we greatly appreciate the funding and facilities provided by RIVM, which made the HT field calibration at the Veenkampen site in Wageningen possible after the mobile campaign.

https://doi.org/10.5194/egusphere-2026-2838
Preprint. Discussion started: 28 July 2026

References

Asman, W. A. H., Sutton, M. A., & Schjørring, J. K. (1998). Ammonia: Emission, atmospheric transport and deposition. *New Phytologist*, *139*(1), 27–48. https://doi.org/10.1046/j.1469-8137.1998.00180.x

Brinklow, G., Herreros, J. M., Zeraati Rezaei, S., Doustdar, O., Tsolakis, A., Kolpin, A., & Millington, P. (2023). Non-carbon greenhouse gas emissions for hybrid electric vehicles: Three-way catalyst nitrous oxide and ammonia trade-off. *International Journal of Environmental Science and Technology*, *20*(11), 12521–12532. https://doi.org/10.1007/s13762-023-04848-2

Burgard, D. A., Bishop, G. A., & Stedman, D. H. (2006). Remote sensing of ammonia and sulfur dioxide from on-road light duty vehicles. *Environmental Science and Technology*, *40*(22), 7018–7022. https://doi.org/10.1021/es061161r

Chen, Z. L., Song, W., Hu, C. C., Liu, X. J., Chen, G. Y., Walters, W. W., Michalski, G., Liu, C. Q., Fowler, D., & Liu, X. Y. (2022). Significant contributions of combustion-related sources to ammonia emissions. *Nature Communications, 13*, 7710. https://doi.org/10.1038/s41467-022-35381-4

Dai, W., Wang, S., Zhang, S., Zhu, J., Gu, C., Sun, Z., Xue, R., & Zhou, B. (2024). A new portable open-path instrument for ambient NH_3 and on-road emission measurements. *Journal of Environmental Sciences (China)*, *136*, 606–614. https://doi.org/10.1016/j.jes.2023.01.017

Delre, A., Hensen, A., Velzeboer, I., Van Den Bulk, P., Edjabou, M. E., & Scheutz, C. (2022). Methane and ethane emission quantifications from onshore oil and gas sites in Romania, using a tracer gas dispersion method. *Elementa: Science of the Anthropocene*, *10*(1), 000111. https://doi.org/10.1525/elementa.2021.000111

Ding, J., Van Der A, R., Eskes, H., Dammers, E., Shephard, M., Wichink Kruit, R., Guevara, M., & Tarrason, L. (2024). Ammonia emission estimates using CrIS satellite observations over Europe. *Atmospheric Chemistry and Physics*, *24*(18), 10583–10599. https://doi.org/10.5194/acp-24-10583-2024

European Environment Agency (EEA). (2023). *Veluwe – Natura 2000 site factsheet*. https://eunis.eea.europa.eu/sites/NL3009016

European Environment Agency (EEA). (2025). *Emissions of air pollutants from transport in Europe*. https://www.eea.europa.eu/en/analysis/indicators/emissions-of-air-pollutants-from

Farren, N. J., Davison, J., Rose, R. A., Wagner, R. L., & Carslaw, D. C. (2020). Underestimated ammonia emissions from road vehicles. *Environmental Science and Technology*, *54*(24), 15689–15697. https://doi.org/10.1021/acs.est.0c05839

https://doi.org/10.5194/egusphere-2026-2838
Preprint. Discussion started: 28 July 2026

Flechard, C. R., Nemitz, E., Smith, R. I., Fowler, D., Vermeulen, A. T., Bleeker, A., Erisman, J. W., Simpson, D., Zhang, L., Tang, Y. S., & Sutton, M. A. (2011). Dry deposition of reactive nitrogen to European ecosystems: A comparison of inferential models across the NitroEurope network. *Atmospheric Chemistry and Physics*, *11*(6), 2703–2728. https://doi.org/10.5194/acp-11-2703-2011

Fowler, D., Pitcairn, C. E. R., Sutton, M. A., Flechard, C., Loubet, B., Coyle, M., & Munro, R. C. (1998). The mass budget of atmospheric ammonia in woodland within 1 km of livestock buildings. *Environmental Pollution*, *102*(1), 343–348. https://doi.org/10.1016/S0269-7491(98)80053-5

Golston, L. M., Pan, D., Sun, K., Tao, L., Zondlo, M. A., Eilerman, S. J., Peischl, J., Neuman, J. A., & Floerchinger, C. (2020). Variability of ammonia and methane emissions from animal feeding operations in Northeastern Colorado. *Environmental Science and Technology*, *54*(18), 11015–11024. https://doi.org/10.1021/acs.est.0c00301

Gyldenkærne, S., Ambelas Skjøth, C., Hertel, O., & Ellermann, T. (2005). A dynamical ammonia emission parameterization for use in air pollution models. *Journal of Geophysical Research: Atmospheres*, *110*(D7), 2004JD005459. https://doi.org/10.1029/2004JD005459

Hensen, A., Loubet, B., Mosquera, J., Van Den Bulk, W. C. M., Erisman, J. W., Dämmgen, U., Milford, C., Löpmeier, F. J., Cellier, P., Mikuška, P., & Sutton, M. A. (2009). Estimation of NH_3 emissions from a naturally ventilated livestock farm using local-scale atmospheric dispersion modelling. *Biogeosciences*, *6*(12), 2847–2860. https://doi.org/10.5194/bg-6-2847-2009

IPCC. (2006). *2006 IPCC Guidelines for National Greenhouse Gas Inventories*. Institute for Global Environmental Strategies (IGES). https://www.ipcc-nggip.iges.or.jp/public/2006gl/

Jiang, H., Zhang, H., Zhao, H., Fu, M., Wang, Y., Wu, X., Yang, X., Ji, J., Yin, H., & Ding, Y. (2023). Exhaust aftertreatment device-derived ammonia emissions from conventional and hybrid light-duty gasoline vehicles over different driving cycles. *Journal of Hazardous Materials*, *458*, 131914. https://doi.org/10.1016/j.jhazmat.2023.131914

Jiang, J., Stevenson, D. S., Uwizeye, A., Tempio, G., Falcucci, A., Casu, F., and Sutton, M. A.(2025). A dynamical process-based model for quantifying global agricultural ammonia emissions – AMmonia–CLIMate v1.0 (AMCLIM v1.0) – Part 2: Livestock farming. *Geoscientific Model Development, 18*, 5051–5099, https://doi.org/10.5194/gmd-18-5051-2025

https://doi.org/10.5194/egusphere-2026-2838
Preprint. Discussion started: 28 July 2026

Kean, A. J., Littlejohn, D., Ban-Weiss, G. A., Harley, R. A., Kirchstetter, T. W., & Lunden, M. M. (2009). Trends in on-road vehicle emissions of ammonia. *Atmospheric Environment*, *43*(8), 1565–1570. https://doi.org/10.1016/j.atmosenv.2008.09.085

Kumar, P., Broquet, G., Hauglustaine, D., Beaudor, M., Clarisse, L., Van Damme, M., Coheur, P., Cozic, A., Zheng, B., Romero, B. R., Delavois, A., & Ciais, P. (2025). Global atmospheric inversion of the anthropogenic NH_3 emissions over 2019–2022 using the LMDZ-INCA chemistry transport model and the IASI NH_3 observations. *Atmospheric Chemistry and Physics*, *25*(19), 12379–12407. https://doi.org/10.5194/acp-25-12379-2025

Lemes, Y. M., Häni, C., Kamp, J. N., & Feilberg, A. (2023). Evaluation of open-and closed-path sampling systems for the determination of emission rates of NH_3 and CH_4 with inverse dispersion modeling. *Atmospheric Measurement Techniques*, *16*(5), 1295–1309. https://doi.org/10.5194/amt-16-1295-2023

Lessmann, M., Kros, H., Walvoort, D., Voogd, J. C., Renaud, L., & Cals, T. (2025). Uncertainties in nitrogen application from manure and synthetic fertilizers and ammonia emissions from agriculture in the Netherlands across different spatial scales. *Nutrient Cycling in Agroecosystems*, *131*(1), 141–164. https://doi.org/10.1007/s10705-025-10410-y

Li, S., Dammers, E., Segers, A., & Erisman, J. W. (2025). Local-scale inversion of agricultural ammonia emissions: A case study on Schiermonnikoog, the Netherlands. *Atmospheric Chemistry and Physics*, *25*(21), 15593–15611. https://doi.org/10.5194/acp-25-15593-2025

Li, S., Liu, T., Song, W., Pei, C., Huang, Z., Wang, Y., Chen, Y., Yan, J., Zhang, R., Zhang, Y., & Wang, X. (2021). Emission factors of ammonia for on-road vehicles in urban areas from a tunnel study in south China with laser-absorption based measurements. *Environmental Pollution*, *280*, 116972. https://doi.org/10.1016/j.envpol.2021.116972

Lichtfouse, E. (Ed.). (2012). *Agroecology and strategies for climate change*. Springer. https://doi.org/10.1007/978-94-007-1905-7

Liu, S., Proudman, J., & Mitloehner, F. M. (2021). Rethinking methane from animal agriculture. *CABI Agriculture and Bioscience*, *2*(1), 22. https://doi.org/10.1186/s43170-021-00041-y

Liu, Z., Liu, Y., Murphy, J., & Maghirang, R. (2017). Ammonia and methane emission factors from cattle operations expressed as losses of dietary nutrients or energy. *Agriculture*, *7*(3), 16. https://doi.org/10.3390/agriculture7030016

https://doi.org/10.5194/egusphere-2026-2838
Preprint. Discussion started: 28 July 2026

764 Lô, S., Dohmen, W., Heederik, D., Weijers, E., Van Schothorst, I., Bleeker, A., Vermeulen, R., & Hoek, G.
765 (2025). Spatial and temporal variability of atmospheric ammonia using a dense network in an area with
766 livestock, residential and natural environments intertwined. *Atmospheric Environment*, *360*, 121394.
767 https://doi.org/10.1016/j.atmosenv.2025.121394
768 Luo, L., Luo, B., & Tai, A. P. K. (2025). Reactive nitrogen from agriculture: a review of emissions, air quality,
769 and climate impacts. *Current Pollution Reports*, *11*(41), 1-23. https://doi.org/10.1007/s40726-025-
770 00360-y
771 Maazallahi, H. (2022). *Detection, attribution and quantification of methane emissions using mobile*
772 *measurement techniques in European cities* (Doctoral dissertation, Utrecht University).
773 https://doi.org/10.33540/1457
774 Mann, H. B., & Whitney, D. R. (1947). On a test of whether one of two random variables is stochastically larger
775 than the other. *The Annals of Mathematical Statistics*, *18*(1), 50–60.
776 https://doi.org/10.1214/aoms/1177730491
777 McCabe, M. E., Pollack, I. B., Fischer, E. V., Steinmann, K. M., & Caulton, D. R. (2023). Technical note:
778 Isolating methane emissions from animal feeding operations in an interfering location. *Atmospheric*
779 *Chemistry and Physics*, *23*(13), 7479–7494. https://doi.org/10.5194/acp-23-7479-2023
780 Miller, D. J., Sun, K., Tao, L., Pan, D., Zondlo, M. A., Nowak, J. B., Liu, Z., Diskin, G., Sachse, G., Beyersdorf,
781 A., Ferrare, R., & Scarino, A. J. (2015). Ammonia and methane dairy emission plumes in the San
782 Joaquin valley of California from individual feedlot to regional scales. *Journal of Geophysical*
783 *Research*, *120*(18), 9718–9738. https://doi.org/10.1002/2015JD023241
784 Mønster, J. G., Samuelsson, J., Kjeldsen, P., Rella, C. W., & Scheutz, C. (2014). Quantifying methane emission
785 from fugitive sources by combining tracer release and downwind measurements – A sensitivity analysis
786 based on multiple field surveys. *Waste Management*, *34*(8), 1416–1428.
787 https://doi.org/10.1016/j.wasman.2014.03.025
788 Moyes, A. B., dos Santos, A. L. D., Reichl, K., & Biraud, S. C. (2025). Dense and diverse regional methane
789 sources characterized using a tiered, dual-tracer measurement strategy. *Atmospheric Environment*, *354*,
790 121270. https://doi.org/10.1016/j.atmosenv.2025.121270
791 Nair, A. A., & Yu, F. (2020). Quantification of atmospheric ammonia concentrations: A review of its
792 measurement and modeling. *Atmosphere*, *11*(10). https://doi.org/10.3390/atmos11101092

https://doi.org/10.5194/egusphere-2026-2838
Preprint. Discussion started: 28 July 2026

Park, T., Singh, R., Ban, J., Kim, K., Park, G., Kang, S., Choi, S., Song, J., Yu, D. G., Bae, M. S., Ahn, J., Jung, H. J., Lim, Y. J., Kim, H. W., Hwang, T. K., Choi, Y. J., Kim, S. Y., Kim, H. S., Chang, Y. W., … Lee, T. (2023). Seasonal and regional variations of atmospheric ammonia across the South Korean Peninsula. *Asian Journal of Atmospheric Environment*, *17*(6).1-11. https://doi.org/10.1007/s44273-023-00008-7

Pasquill, F., & Smith, F. B. (1983). *Atmospheric Diffusion* (3rd ed.). John Wiley & Sons, Ltd.

Pu, W., Sheng, J., Tian, P., Huang, M., Liu, X., Collett, J. L., Li, Z., Zhao, X., He, D., Dong, F., Zhang, N., Quan, W., Qiu, Y., Song, Y., Lin, W., Pan, Y., & Ma, Z. (2023). On-road mobile mapping of spatial variations and source contributions of ammonia in Beijing, China. *Science of the Total Environment*, *864*, 160869. https://doi.org/10.1016/j.scitotenv.2022.160869

Rijksdienst voor Ondernemend Nederland. (n.d.-a). *Kernregistratie Dierverblijven (KRD)*. Retrieved March 19, 2026, from https://viewer.igoview.nl/kaartviewer

Rijksdienst voor Ondernemend Nederland. (n.d.-b). *Regeling ammoniak en veehouderij (RAV): Stalbeschrijvingen en emissiefactoren*. Retrieved March 19, 2026, from https://iplo.nl/regelgeving/regels-voor-activiteiten/dierenverblijven/systeembeschrijvingen-stallen/

National Institute for Public Health and the Environment (RIVM). (2023). *Monitor stikstofdepositie in Natura 2000 gebieden 2023* (Report No. 2023-0239). https://www.rivm.nl/bibliotheek/rapporten/2023-0239.pdf

National Institute for Public Health and the Environment (RIVM) & Statistics Netherlands (CBS). (2024). *Emissieregistratie: Regional emissions to air in the Netherlands*. https://www.emissieregistratie.nl/

Ruyssenaars, P. G., Coenen, P. W. H. G., Rienstra, J. D., Zijlema, P. J., Arets, E. J. M. M., Baas, K., Dröge, R., Geilenkirchen, G., 't Hoen, M., Honig, E., van Huet, B., van Huis, E. P., Koch, W. W. R., te Molder, R. M., Montfoort, J. A., van der Zee, T., & van Zanten, M. C. (2020). *Greenhouse gas emissions in the Netherlands 1990–2018: National inventory report 2020* (RIVM Report No. 2020-0031). https://www.rivm.nl/bibliotheek/rapporten/2020-0031.pdf

Saha, C. K., Ammon, C., Berg, W., Fiedler, M., Loebsin, C., Sanftleben, P., Brunsch, R., & Amon, T. (2014). Seasonal and diel variations of ammonia and methane emissions from a naturally ventilated dairy building and the associated factors influencing emissions. *Science of the Total Environment*, *468–469*, 53–62. https://doi.org/10.1016/j.scitotenv.2013.08.015

Schulte, R. B., Van Zanten, M. C., Van Stratum, B. J. H., & De Arellano, J. V. G. (2022). Assessing the representativity of NH_3 measurements influenced by boundary-layer dynamics and the turbulent

https://doi.org/10.5194/egusphere-2026-2838
Preprint. Discussion started: 28 July 2026

dispersion of a nearby emission source. *Atmospheric Chemistry and Physics*, *22*(12), 8241–8257. https://doi.org/10.5194/acp-22-8241-2022

Shan, N., Wei, S., Fan, Y., Tong, Y., Wang, C., Hu, X., Liu, B., Wang, W., & Shan, N. (2025). Seasonal characteristics on the ammonia emissions of a typical large-scale pig farm in the Yangtze River Delta, China. *Atmospheric Environment: X*, *27*, 100354. https://doi.org/10.1016/j.aeaoa.2025.100354

Shen, J., Chen, D., Bai, M., Sun, J., Coates, T., Lam, S. K., & Li, Y. (2016). Ammonia deposition in the neighbourhood of an intensive cattle feedlot in Victoria, Australia. *Scientific Reports*, *6*, 1–9. https://doi.org/10.1038/srep32793

Sherman, J., Young, E., Jokela, W., & Kieke, B. (2022). Manure application timing and incorporation effects on ammonia and greenhouse gas emissions in corn. *Agriculture*, *12*(11), 1952. https://doi.org/10.3390/agriculture12111952

Sommer, S. G., Génermont, S., Cellier, P., Hutchings, N. J., Olesen, J. E., & Morvan, T. (2003). Processes controlling ammonia emission from livestock slurry in the field. *European Journal of Agronomy*, *19*(4), 465–486. https://doi.org/10.1016/S1161-0301(03)00037-6

Statistics Netherlands (CBS). (2023). *Emissions to air from road transport, the Netherlands*. https://www.cbs.nl/nl-nl/cijfers/detail/85347NED

Statistics Netherlands (CBS). (2024). *Emissions to air from agriculture*. https://www.cbs.nl/nl-nl/longread/aanvullende-statistische-diensten/2024/emissies-van-de-nederlandse-landbouw-naar-productgroepen-erratum/2-emissies-naar-lucht-door-de-landbouw

Stelwagen, U., & Ligterink, N. E. (2015). *NH_3 emission factors for road transport* (TNO Report No. 2015 R11005). https://publications.tno.nl/publication/34620128/gqEWSG/TNO-2015-R11005.pdf

Suarez-Bertoa, R., Zardini, A. A., Lilova, V., Meyer, D., Nakatani, S., Hibel, F., Ewers, J., Clairotte, M., Hill, L., & Astorga, C. (2015). Intercomparison of real-time tailpipe ammonia measurements from vehicles tested over the new world-harmonized light-duty vehicle test cycle (WLTC). *Environmental Science and Pollution Research*, *22*(10), 7450–7460. https://doi.org/10.1007/s11356-015-4267-3

Sun, K., Tao, L., Miller, D. J., Khan, M. A., & Zondlo, M. A. (2014). On-road ammonia emissions characterized by mobile, open-path measurements. *Environmental Science and Technology, 48*(7), 3943–3950. https://pubs.acs.org/doi/10.1021/es4047704

Sun, K., Tao, L., Miller, D. J., Pan, D., Golston, L. M., Zondlo, M. A., Griffin, R. J., Wallace, H. W., Leong, Y. J., Yang, M. M., Zhang, Y., Mauzerall, D. L., & Zhu, T. (2017). Vehicle emissions as an important

https://doi.org/10.5194/egusphere-2026-2838
Preprint. Discussion started: 28 July 2026

urban ammonia source in the United States and China. *Environmental Science and Technology, 51*(4), 2472–2481. https://doi.org/10.1021/acs.est.6b02805

Swart, D., Zhang, J., van der Graaf, S., Rutledge-Jonker, S., Hensen, A., Berkhout, S., Wintjen, P., van der Hoff, R., Haaima, M., Frumau, A., van den Bulk, P., Schulte, R., van Zanten, M., & van Goethem, T. (2023). Field comparison of two novel open-path instruments that measure dry deposition and emission of ammonia using flux-gradient and eddy covariance methods. *Atmospheric Measurement Techniques, 16*, 529–546. https://doi.org/10.5194/amt-16-529-2023

Tettenborn, J., Zavala-Araiza, D., Stroeken, D., Maazallahi, H., van der Veen, C., Hensen, A., Velzeboer, I., van den Bulk, P., Vogel, F., Gillespie, L., Ars, S., France, J., Lowry, D., Fisher, R., & Röckmann, T. (2025). Improving consistency in methane emission quantification from the natural gas distribution systems across measurement devices. *Atmospheric Measurement Techniques*, *18*(14), 3569–3584. https://doi.org/10.5194/amt-18-3569-2025

Tong, X., Zhao, Z., Hensen, A., Bruin, G. J., van Heuven, S., Scheeren, B., Hutjes, R., & Chen, H. (2025). Toward reconciling bottom-up and top-down estimates of N_2O and CH_4 emissions in Rotterdam. *Journal of Geophysical Research: Atmospheres*, *130*(21). https://doi.org/10.1029/2025JD044365

Turner, D. B. (1994). *Workbook of atmospheric dispersion estimates: An introduction to dispersion modeling*. CRC Press.

Twigg, M. M., Berkhout, A. J. C., Cowan, N., Crunaire, S., Dammers, E., Ebert, V., Gaudion, V., Haaima, M., John, A., Jones, K., Kamps, J., Kentisbeer, J., Kupper, M., Leeson, J., Leuenberger, C., Luettenschwager, S., Makkonen, U., Martin, D., Missler, J., … Niederhauser, J. (2022). Intercomparison of in situ measurements of ambient NH_3: instrument performance and application under field conditions. *Atmospheric Measurement Techniques*, 15, 6755–6787. https://doi.org/10.5194/amt-15-6755-2022

Van Der Graaf, S., Dammers, E., Segers, A., Kranenburg, R., Schaap, M., Shephard, M. W., & Erisman, J. W. (2022). Data assimilation of CrIS NH_3 satellite observations for improving spatiotemporal NH_3 distributions in LOTOS-EUROS. *Atmospheric Chemistry and Physics*, *22*(2), 951–972. https://doi.org/10.5194/acp-22-951-2022

Van der Net, L., Staats, N., Coenen, P. W. H. G., Rienstra, J. D., Zijlema, J. D. P. J., Arets, E. J. M. M., Baas, K., van Baren, S. A., Dröge, R., Geertjes, K., Honig, E., van Huet, B., te Molder, R. A. B., Montfoort, J. A., van der Zee, T. C., & van Zanten, M. C. (2024). *Greenhouse gas emissions in the Netherlands 1990-*

https://doi.org/10.5194/egusphere-2026-2838
Preprint. Discussion started: 28 July 2026

2022: *National Inventory Report 2024* (RIVM Report No. 2024-0017). https://www.rivm.nl/bibliotheek/rapporten/2024-0017.pdf

Van Pul, A., Van Jaarsveld, H., Van Der Meulen, T., & Velders, G. (2004). Ammonia concentrations in the Netherlands: Spatially detailed measurements and model calculations. *Atmospheric Environment*, *38*(24), 4045–4055. https://doi.org/10.1016/j.atmosenv.2004.03.051

Van Wijk, D., Raben, C. R., Erbrink, H. J., Heederik, D. J. J., & Dohmen, W. (2025). Effects of different ammonia emission reduction strategies from livestock farming on ambient ammonia concentrations in nature areas: A series of scenario analyses. *Atmospheric Environment: X*, *28*, 100370. https://doi.org/10.1016/j.aeaoa.2025.100370

Van Zanten, M. C., Wichink Kruit, R. J., Hoogerbrugge, R., Van der Swaluw, E., & van Pul, W. A. J. (2017). Trends in ammonia measurements in the Netherlands over the period 1993–2014. *Atmospheric Environment*, *148*, 352–360. https://doi.org/10.1016/j.atmosenv.2016.11.007

Vechi, N. T., Mellqvist, J., Samuelsson, J., Offerle, B., & Scheutz, C. (2023). Ammonia and methane emissions from dairy concentrated animal feeding operations in California, using mobile optical remote sensing. *Atmospheric Environment*, *293*, 119448. https://doi.org/10.1016/j.atmosenv.2022.119448

Velthof, G. L., Van Bruggen, C., Groenestein, C. M., De Haan, B. J., Hoogeveen, M. W., & Huijsmans, J. F. M. (2012). A model for inventory of ammonia emissions from agriculture in the Netherlands. *Atmospheric Environment*, *46*, 248–255. https://doi.org/10.1016/j.atmosenv.2011.09.075

Velzeboer, I., Zhang, J., Van de Bulk, W. C. M., & Hensen, A. (2024). *Landfill Methane Measurements 2022-2023* (TNO Report No. 2023 R11711). https://publications.tno.nl/publication/34642182/kT1ClO/TNO-2023-R11711.pdf

Vinković, K., Andersen, T., de Vries, M., Kers, B., van Heuven, S., Peters, W., Hensen, A., van den Bulk, P., & Chen, H. (2022). Evaluating the use of an Unmanned Aerial Vehicle (UAV)-based active AirCore system to quantify methane emissions from dairy cows. *Science of the Total Environment*, *831*, 154898. https://doi.org/10.1016/j.scitotenv.2022.154898

Vogel, F., Ars, S., Wunch, D., Lavoie, J., Gillespie, L., Maazallahi, H., Röckmann, T., Nęcki, J., Bartyzel, J., Jagoda, P., Lowry, D., France, J., Fernandez, J., Bakkaloglu, S., Fisher, R., Lanoiselle, M., Chen, H., Oudshoorn, M., Yver-Kwok, C., … Calcan, A. (2024). Ground-based mobile measurements to track urban methane emissions from natural gas in 12 cities across eight countries. *Environmental Science and Technology*, *58*(5), 2271–2281. https://doi.org/10.1021/acs.est.3c03160

https://doi.org/10.5194/egusphere-2026-2838
Preprint. Discussion started: 28 July 2026

913 Wang, K., Kang, P., LU, Y., Zheng, X., Liu, M., Lin, T. J., Butterbach-Bahl, K., & Wang, Y. (2021). An open-
914 path ammonia analyzer for eddy covariance flux measurement. *Agricultural and Forest Meteorology*,
915 *308–309*, 108570. https://doi.org/10.1016/j.agrformet.2021.108570
916 Wang, Y., Wen, Y., Zhang, S., Zheng, G., Zheng, H., Chang, X., Huang, C., Wang, S., Wu, Y., & Hao, J.
917 (2023). Vehicular ammonia emissions significantly contribute to urban $PM_{2.5}$ pollution in two Chinese
918 megacities. *Environmental Science and Technology*, *57*(7), 2698–2705.
919 https://doi.org/10.1021/acs.est.2c06198
920 Wen, M., Wang, X., Zhao, H., Feng, J., Xu, X., Ge, Z., Lyu, L., Wang, C., & Ge, Y. (2025). Ammonia emissions
921 from series and series-parallel plug-in hybrid electric vehicles under real driving condition. *Journal of*
922 *Hazardous Materials*, *495*, 138910. https://doi.org/10.1016/j.jhazmat.2025.138910
923 Wen, Y., Zhang, S., Wu, Y., & Hao, J. (2023). Vehicular ammonia emissions: An underappreciated emission
924 source in densely populated areas. *Atmospheric Chemistry and Physics*, *23*(6), 3819–3828.
925 https://doi.org/10.5194/acp-23-3819-2023
926 Wever, D., Bolech, M., Coenen, P. W. H. G., Dellaert, S. N. C., & Dröge, R., Geilenkirchen, G., Honig, E., van
927 Huet, B., Kosterman, M., van Mill, S. E. H., van Zanten, M. C., van der Zee, T. (2024). *Informative*
928 *Inventory Report 2024: Emissions of transboundary air pollutants in the Netherlands 1990–2022*
929 (RIVM report No. 2024-0018). https://doi.org/10.21945/RIVM-2024-0018
930 Wietzel, J. B., Korben, P., Hoheisel, A., & Schmidt, M. (2025). Best practices and uncertainties in CH_4 emission
931 quantification: Employing mobile measurements and Gaussian plume modelling at a biogas plant.
932 *Atmospheric Measurement Techniques, 18*, 4631–4645. https://doi.org/10.5194/amt-18-4631-2025
933 Yacovitch, T. I., Herndon, S. C., Pétron, G., Kofler, J., Lyon, D., Zahniser, M. S., & Kolb, C. E. (2015). Mobile
934 laboratory observations of methane emissions in the Barnett Shale region. *Environmental Science and*
935 *Technology*, *49*(13), 7889–7895. https://doi.org/10.1021/es506352j
936 Yang, F., Han, Y., Bi, H., Wei, X., Luo, W., & Li, G. (2022). Ammonia emissions and their key influencing
937 factors from naturally ventilated dairy farms. *Chemosphere*, *307*, 135747.
938 https://doi.org/10.1016/j.chemosphere.2022.135747
939 Yang, J., Xu, Z., Xia, Z., Pei, X., Yang, Y., Qiu, B., Zhao, S., Zhang, Y., & Wang, Z. (2025). Locating and
940 quantifying CH_4 sources within a wastewater treatment plant based on mobile measurements.
941 *Atmospheric Chemistry and Physics*, *25*(8), 4571–4585. https://doi.org/10.5194/acp-25-4571-2025

https://doi.org/10.5194/egusphere-2026-2838
Preprint. Discussion started: 28 July 2026

Yi, W., Liu, G., Wang, M., Wang, J., Chen, D., & Shen, J. (2025). Increased nitrogen deposition and airborne particulate matter pollution in the vicinity of intensive animal farms caused by ammonia emissions. *Agriculture, Ecosystems & Environment*, *387*, 109634. https://doi.org/10.1016/j.agee.2025.109634

Zavala, M., Herndon, S. C., Wood, E. C., Jayne, J. T., Nelson, D. D., Trimborn, A. M., Dunlea, E., Knighton, W. B., A. Mendoza, Allen, D. T., Kolb, C. E., Molina, M. J., & Molina, L. T. (2009). Comparison of emissions from on-road sources using a mobile laboratory under various driving and operational sampling modes. *Atmospheric Chemistry and Physics*, *9*(1), 1–14. https://doi.org/10.5194/acp-9-1-2009

Zhang, J., Bronsveld, P. C. P., Hensen, A., van Mansom, H., Van Den Bulk, P., & Velzeboer, I. (2025). Traceable calibration of open- and closed-path ammonia analyzers using the VSL RGM system and its impact on livestock emission uncertainty (TNO Report No. 2024 R12917). https://publications.tno.nl/publication/34645262/kM5oVotk/TNO-2024-R12917.pdf

Zhuang, M., Shan, N., Wang, Y., Caro, D., Fleming, R. M., & Wang, L. (2020). Different characteristics of greenhouse gases and ammonia emissions from conventional stored dairy cattle and swine manure in China. *Science of The Total Environment*, *722*, 137693. https://doi.org/10.1016/j.scitotenv.2020.137693